

PROMISE

Protective Range-Optimized Missile Imitating Supersonic Entities

It's Not a Threat, It's a PROMISE

AIAA
SHAPING THE FUTURE OF AEROSPACE

Georgia Tech Aerospace Systems Design Laboratory

*Design Proposed By:
Aerospace Systems Design Laboratory
Georgia Institute of Technology, Atlanta, Georgia*



Dr. Dimitri Mavris
Faculty Advisor

Dimitri Mavris



Dr. Bradford Robertson
Research Advisor

Bradford Robertson



Mr. Andrew Yatsko
Research Advisor
Air-Breathing Propulsion

Andrew J. Yatsko



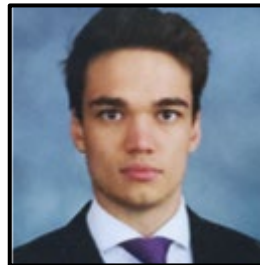
Sarah Malak
Propulsion
ASDL
AIAA # 1098269

Sarah Malak



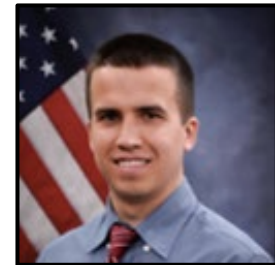
Zach Parham
Propulsion
Undergraduate
AIAA # 775584

Zach Parham



Andrej Šulek
Propulsion
Undergraduate
AIAA # 1098306

Andrej Šulek



Nate Simon
Trajectory
ASDL
AIAA # 952743

Nathan Simon



Rosa Bonilla
Structures
Graduate
AIAA # 1070303

Rosa Bonilla



Nikolay Tranakiev
Structures
Undergraduate
AIAA # 1098445

Nikolay Tranakiev



Scott Nealon
Aerodynamics
ASDL
AIAA # 643141

Scott Nealon



Jessica Grimmert
Aerodynamics
Undergraduate
AIAA # 1098445

Jessica Grimmert

Design for a Supersonic Aerial Target

*Sarah Malak¹, Nathan Simon¹, Scott Nealon¹, Rosa Bonilla²,
Jessica Grimmet³, Zachary Parham³, Andrej Šulek³, Nikolay Tranakiev³*
Aerospace Systems Design Laboratory, Georgia Institute of Technology, Atlanta, GA, 30332, USA

The purpose of this report is to outline the design of a supersonic aerial target, capable of both a high diver and sea skimming profile, in response to the American Institute of Aeronautics and Astronautics (AIAA) 2019-2020 Graduate Team Missile Systems Design Competition Request for Proposal.

I. Nomenclature

A_c	= stage cross sectional area	T_c	= combustion temperature ratio
a	= speed of sound	T	= thrust
C_D	= coefficient of drag	t	= frame thickness
C_L	= coefficient of lift	V	= velocity
C_{ma}	= pitching moment coefficient	W	= weight
g	= gravitational acceleration	α	= angle of attack
H_f	= heating value	γ	= specific heat ratio
I_{SP}	= specific impulse	γ_{flight}	= flight path angle
M	= Mach number	δ	= turning angle
m	= mass	ρ	= air density
P_c	= chamber pressure	σ	= stress
R	= body radius	θ_{shock}	= shock angle
S	= reference area	θ_{pitch}	= pitch angle

¹ Graduate Research Assistant, Aerospace Systems Design Laboratory (Georgia Tech), AIAA Student Member

² Graduate Student, Georgia Tech, AIAA Student Member

³ Undergraduate Student, Georgia Tech, AIAA Student Member

II. Table of Contents

I.	Nomenclature.....	3
II.	Table of Contents.....	4
III.	List of Tables.....	7
IV.	List of Figures.....	9
V.	Executive Summary.....	12
VI.	Introduction	12
A.	Project Introduction	12
B.	Motivation and Existing Systems	13
VII.	Requirements	14
A.	Concept of Operations	14
B.	Explicit Requirements	15
C.	Derived Requirements	16
1.	Propulsive Efficiency.....	16
2.	Lift, Vectored Thrust Production.....	16
3.	Propulsion Considerations for Cruise	16
4.	Guidance, Navigation, and Control System.....	17
5.	Structure Capable of Withstanding Loads	17
VIII.	Approach	18
A.	Motivation	18
B.	Geometry	19
1.	External Geometry.....	20
2.	Internal Geometry	22
C.	Propulsion.....	23
1.	Air-Breathing Propulsion.....	23
2.	Boost Phase.....	27
3.	Propellant Section	29

- D. Weights & Structures.....29
 - 1. Weights and Center of Gravity29
 - 2. Structural Analysis.....31
 - 3. Material Selection32
 - 1. Factor of Safety Calculation33
- E. Aerodynamics34
- F. Trajectory.....36
 - 1. Equations of Motion36
 - 2. Aerodynamics37
 - 3. Propulsion38
 - 4. Trajectory Propagation38
 - 5. Midcourse Terminal Approach39
 - 6. Circular Error Probable.....39
- G. Cost and Manufacturing Modeling40
- H. Maintenance and Safety Considerations40
- IX. Design of Experiments.....41
 - A. Body Sizing Ranging Experiment41
 - B. Solid Booster Ranging Experiment51
 - C. Final Design of Experiments53
 - D. Final Design Changes59
- X. Results59
 - A. Geometry60
 - B. Weights and Structures61
 - 1. Weight and Center of Gravity.....61
 - 2. Stress Analysis.....62
 - C. Trajectory.....63
 - 1. High Dive Flight Profile63
 - 2. Sea Skimming Flight Profile.....67

3.	Varied Operating Conditions	70
4.	Trajectory Summary	71
D.	Cost and Operations	71
XI.	Conclusion	73
A.	Specification Compliance	73
XII.	Acknowledgments	76
XIII.	References	76

III. List of Tables

Table 1. Executive summary.....	12
Table 2. Explicit requirements.....	16
Table 3. Derived requirements.....	17
Table 4. Defaulted geometric parameters.....	22
Table 5. Component weight estimation.....	30
Table 6. Variables and ranges for body sizing ranging experiment.....	42
Table 7. Variables and ranges for first design of experiments.....	42
Table 8. Number of vehicles meeting constraints for body sizing ranging experiment.....	49
Table 9. Parameter range updates from body sizing ranging experiment.....	50
Table 10. Number of vehicles meeting constraints for body sizing ranging experiment with updated ranges.....	50
Table 11. Variables and ranges for body sizing ranging experiment.....	51
Table 12. Parameter range updates from solid booster ranging experiment.....	52
Table 13. Variables and ranges for first design of experiments.....	53
Table 14. Number of vehicles meeting pre-trajectory constraints for final selection DOE.....	53
Table 15. Number of vehicles meeting boost constraints for final selection DOE.....	54
Table 16. Number of vehicles meeting range constraints for final DOE.....	55
Table 17. TOPSIS positive and negative ideal solutions.....	57
Table 18. Top 5 TOPSIS alternatives.....	58
Table 19. Final Design Changes.....	59
Table 20. DOE parameters of the ASDL-1776.....	60
Table 21. Remaining geometric parameters of the ASDL-1776.....	60
Table 22. Weight and CG results.....	61
Table 23. Stress analysis results.....	63
Table 24. Performance compared to Brahmos and trajectory requirements.....	71
Table 25. Operational costs.....	72
Table 26. Total life cycle costs.....	73

Table 27. Compliance color chart74

Table 28. Specification Compliance74

IV. List of Figures

Fig. 1. Missile design environment N^2 diagram.....	19
Fig. 2. Sample geometric missile layouts.....	20
Fig. 3. Sample internal packing of missile.....	23
Fig. 4. NPSS ramjet block diagram.....	24
Fig. 5. Specific impulse modeling of ramjet.....	26
Fig. 6. Visualization of geometric burn algorithm.....	27
Fig. 7. Core geometries handled by SMAC 3.1.....	28
Fig. 8. Lift coefficient (C_L) and drag coefficient (C_D) surfaces generated by Missile Datcom.....	35
Fig. 9. Pitching moment coefficient derivative with angle of attack ($C_{m\alpha}$).....	35
Fig. 10. Maximum range cruise trajectory.....	39
Fig. 11. Early terminal dive trajectory.....	39
Fig. 12. Scatterplot matrix of missile length, missile fineness, and missile diameter highlighting payload diameter constraint.....	43
Fig. 13. Scatterplot matrix of missile length, missile fineness, nose fineness, and center body length highlighting fuel volume constraint.....	44
Fig. 14. Scatterplot matrix of missile length, missile fineness, missile diameter, and $C_{m\alpha}$ highlighting stability constraint.....	45
Fig. 15. Scatterplot matrix of wing area, wing trailing edge percentage, tail area, tail trailing edge percentage, and $C_{m\alpha}$ highlighting stability constraint.....	46
Fig. 16. Scatterplot matrix of missile length, missile fineness ratio, missile diameter, and boost Mach number highlighting boost constraint.....	47
Fig. 17. Scatterplot matrix of solid booster stage length ratio, solid booster grain inner diameter ratio, solid booster stage length, and boost Mach number highlighting boost constraint.....	48
Fig. 18. Scatterplot matrix of missile performance metrics against significant DOE parameters.....	49
Fig. 19. Scatterplot matrix of missile performance metrics against significant DOE parameters.....	52
Fig. 20. Scatterplot matrix of missile performance metrics against significant DOE parameters.....	56

Fig. 21. Scatterplot matrix of missile performance metrics colored by TOPSIS performance.	58
Fig. 22. ASDL-1776 PROMISE visual rendering.....	60
Fig. 23. Launch CG variation with payload weight.	62
Fig. 24. Solid booster burnout CG variation with payload weight.....	62
Fig. 25. Solid booster drop CG variation with payload weight.....	62
Fig. 26. Liquid fuel depletion CG variation with payload weight.....	62
Fig. 27. Time history of high dive flight altitude.....	64
Fig. 28. Time history of high dive range.....	64
Fig. 29. Time history of high dive velocity.....	64
Fig. 30. Time history of high dive Mach number.	64
Fig. 31. Time history of high dive overall weight.....	65
Fig. 32. Time history of high dive fuel mass flow.	65
Fig. 33. High dive thrust to weight and lift to drag ratios during boost phase.	66
Fig. 34. High dive altitude vs range.	66
Fig. 35. High dive time history of flight angle of attack, pitch angle, and flight path angle.....	66
Fig. 36. High dive aerodynamic and propulsive forces.....	66
Fig. 37. Flight trajectory for high dive.....	67
Fig. 38. Mach number for high dive.	67
Fig. 39. Time history of sea skimming flight altitude.....	68
Fig. 40. Time history of sea skimming range.....	68
Fig. 41. Time history of sea skimming velocity.....	68
Fig. 42. Time history of sea skimming Mach number.	68
Fig. 43. Time history of sea skimming overall weight.....	69
Fig. 44. Time history of sea skimming fuel mass flow.	69
Fig. 45. Sea skimming thrust to weight and lift to drag ratios during boost phase.	69
Fig. 46. Sea skimming altitude vs range.	69
Fig. 47. Sea skimming time history of flight angle of attack, pitch angle, and flight path angle.....	70
Fig. 48. Sea skimming aerodynamic and propulsive forces.....	70

Fig. 49. High diver flight trajectory for sea level launch altitude.70

Fig. 50. High diver flight trajectory for 3500 ft launch altitude.....70

Fig. 51. Production cost per unit72

V. Executive Summary

Table 1 lists the requirements laid out in the Request for Proposal (RFP) [1], how the ASDL-1776 PROMISE missile performs with respect to each metric, and in which section of the report the analysis of the missile's performance for each metric can be found.

Table 1. Executive summary.

Requirement	Threshold / Objective	Design Value / Method	Analysis Location
Range	60 / 150 nmi	<i>High Diver:</i> 182+ nmi <i>Sea Skimming:</i> 152 nmi	<i>High Diver:</i> Section X.C.1 <i>Sea Skimming:</i> Section X.C.2
Cruise Speed	<i>High Diver:</i> Mach 2.0 – 4.5 <i>Sea Skimming:</i> Mach 2.0 – 3.5	<i>High Diver:</i> Mach 3.25 <i>Sea Skimming:</i> Mach 2.75	<i>High Diver:</i> Section X.C.1 <i>Sea Skimming:</i> Section X.C.2
Cruise Altitude	<i>High Diver:</i> 5000 ft – 65000 ft <i>Sea Skimming:</i> 15 ft – 200 ft	<i>High Diver:</i> 50,000 ft <i>Sea Skimming:</i> 195 ft	<i>High Diver:</i> Section X.C.1 <i>Sea Skimming:</i> Section X.C.2
Impact Speed	<i>High Diver:</i> Mach 0.9 – 3.5 <i>Sea Skimming:</i> Mach 2.0 – 3.5	<i>High Diver:</i> Mach 2.99 <i>Sea Skimming:</i> Mach 2.6	<i>High Diver:</i> Section X.C.1 <i>Sea Skimming:</i> Section X.C.2
Circular Error Probable (CEP)	50 ft	29.5 ft horizontal, 49.2 ft vertical	Section VIII.F.6
Sea Skimming Maneuvers	15 g Lateral Turns 7 g Vertical Turns Maneuver Duration 45 s	Capable of withstanding > 15 g	Section X.B.2
Launch	Altitude: 0 ft – 3500 ft Elevation: 0° - 90°	<i>Capability:</i> 0 ft – 3500 ft <i>High Diver:</i> 45° <i>Sea Skimming:</i> 12.5°	Section X.C.3

VI. Introduction

A. Project Introduction

The report details the final design of the Georgia Institute of Technology's Missile Design team entry to the 2019-2020 AIAA Graduate Team Missile Systems Design Competition. The team consists of first year graduate students and undergraduate students attending the Georgia Institute of Technology. Every year, the AIAA Graduate Team

Missile Systems Design Competition sponsors an intercollegiate competition with a new missile RFP. This year, the RFP calls for a new supersonic aerial target that will be able to develop new air defenses or train defense system operators against possible threats [1]. This system will have to have performance characteristics that are closely representative of the current threat systems that air defenses are designed to engage. The remainder of the report will provide a detailed description of the design process, the down-selection process, and the final design for the Protective Range-Optimized Missile Imitating Supersonic Entities, also known as ASDL-1776 PROMISE.

B. Motivation and Existing Systems

The world market for supersonic cruise missiles is growing, with the Indian-Russian BrahMos leading the competition, and the Chinese Hongda HD-1 currently in development and set to be a close competitor. BrahMos Aerospace is a joint venture between the Defense Research and Development Organization of India and the Military Industrial Consortium “NPO Mashinostroyenia” of Russia. Based on the company’s website, current capabilities of BrahMos include cruise speeds around Mach 3, a flight range of around 150 nmi (though future versions are expected to exceed this), and cruise altitudes ranging from 30 ft to 50,000 ft [2]. These statistics easily exceed the capabilities of all other cruise missiles that are currently on the market. The Chinese Hongda HD-1 is a system that is supposed to be in direct competition with BrahMos, with cruise speeds of up to Mach 3.5 [3]. Based on open-source information, the Hongda HD-1 has completed its first flight test, but there is no information currently available regarding the outcome of this flight test, or further details about the design itself. In December of 2019, BrahMos successfully completed a ground launch from a land-based mobile launcher and an air-launched flight test from a Sukhoi-30 MKI fighter jet [4]

There are some existing target missiles currently in use, serving as surrogates of hostile threats to train air defense systems. One example is the AQM-37 Jayhawk, which first flew in 1961. The AQM-37 Jayhawk is incapable of the sea-skimming profile, presenting a need for the PROMISE missile in order to achieve all necessary mission profiles. Additionally, there is limited production of the AQM-37, which has led to a dwindling supply [5][6]. Another target missile is the GQM-173 Multi-Stage Supersonic Target that was designed to emulate Russia’s SS-N-27 “Sizzler,” and replace the aging fleet of AQM-37 [7]. The GQM-173 only modeled the supersonic sprint phase and cruises at subsonic speeds. This program was canceled in 2015, creating another opening for a new target system [8]. A third existing missile system that has the closest mission profile to the RFP for this design is the GQM-163A Coyote. This

target missile was designed to emulate Russia's P-800 Oinks, the predecessor to the BrahMos missile [9]. The GQM-163A Coyote is capable of both sea skimming and high diver profiles, however, it has a shorter range than comparable threats [10].

From a defense standpoint, the current U.S. missiles being used to train defense systems are highly inferior to the current weapons in operation. Whether defense systems continue to use intercept missiles, artillery guns, or if they transition towards directed energy systems, it is important to be able to train operators against a target that closest resembles the greatest threat. With BrahMos posing as a threat capable of operating from the ground, air, and sea, the BrahMos missile, along with the RFP requirements, will be used to create a basis for performance comparison during the development of the ASDL-1776 PROMISE, the next supersonic aerial target system.

VII. Requirements

A. Concept of Operations

Though ASDL-1776 will have two distinct concepts of operations for each mission profile, they will follow the same general phases of operation, including launch initiation, launch, mid-course cruise, terminal phase, and terminal impact. Prior to launch initiation, the missile will require a transport and erector system for integration and checkout operations. The erector will be a device capable of taking the missile from a horizontal to vertical position, and vice versa. The transporter will be a vehicle with the ability to house and transport the erector and the missile in its horizontal configuration. Once transport is complete, ASDL-1776 will remain in its horizontal configuration for storage. The missile and its solid propellant will be stored in a controlled facility to ensure compatibility with safe storage, transportation, and handling requirements for 10 years without maintenance, as specified by the RFP [1]. Liquid fuel will be stored separately and added prior to launch.

The launch initiation will be triggered by an order sent to a command post. The transporter and erector system will properly position the missile onto a launch rail. Due to the use of a solid rocket booster, the thrust at launch will be sufficient for ASDL-1776 to take flight without assistance from the launch rail. Thus, the length of the launch rail will be 29.5 ft, or roughly equal to the length of the missile itself. The launch rail will be mounted at 45° for the high-altitude profile or 12.5° for the sea skimming profile. The crew members at the command post will initiate launch, load liquid fuel, and configure the Guidance, Navigation, and Control System to either the high-altitude profile or the

sea skimming profile. ASDL-1776 accepts a modular payload, allowing for an alternate payload to be loaded during pre-launch as necessary. The missile will be stored with the standard 500 lbs. full payload.

The launch phase will commence once the booster is ignited and missile ascent begins. Once booster burnout is complete, the missile will eject the booster and transition to the mid-course cruise phase, where the system will remain until it reaches the terminal phase. For the low-altitude profile, the terminal phase will consist of high-g maneuvers. These maneuvers will be initiated by the command post and will continue for up to 45 seconds, followed by terminal impact. In the high-altitude profile, the terminal phase is marked by a high-speed dive, followed by terminal impact.

B. Explicit Requirements

Within the RFP, the AIAA set a list of explicit requirements for this year's missile design, including requirements for both high diver and sea skimming flight profiles, as well as launch system and life cycle management requirements. The range objective is 150 nmi, with a required range threshold of 60 nmi. The missile should have a cruise altitude between 0 ft and 65,000 ft, with the objective of minimizing the launch-to-cruise transition distance. The circular error probable (CEP) must be within 50 ft. For the high diver flight profile, the missile must cruise between 5,000 ft and 65,000 ft, have a cruise speed between Mach 2.0 and Mach 4.5, and terminate with an impact speed of Mach 0.9 to Mach 3.5. For the sea skimming flight profile, the missile must have a cruise altitude between 15 ft and 200 ft, a cruise speed between Mach 2.0 and Mach 3.5, and terminate with an impact speed of Mach 2.0 to Mach 3.5. The sea skimming profile also requires 15 g lateral turn maneuvers and 7 g vertical turn maneuvers with a duration of 45 seconds. The missile payload has a maximum weight of 500 lbs., and there is an additional production requirement of 350 units with 15 development units. Table 2 outlines the explicit requirements contained in the RFP [1].

Table 2. Explicit requirements.

Requirement	Threshold	Objective
Range	60 nmi	150 nmi
	Minimum	Maximum
Cruise Altitude	0 ft	65,000 ft
Cruise Speed	Mach 2.0	High-Diver: Mach 4.5 Sea Skimming: Mach 3.5
Impact Speed	High-Diver: Mach 0.9 Sea Skimming: Mach 2.0	Mach 3.5
Maneuvers	Lateral: 15 g Vertical: 7 g	
CEP	50 ft	
Payload Weight	Up to 500 lbs.	
Production Run	350 Units + 15 Development Units	

C. Derived Requirements

After analyzing the requirements defined in the RFP, there were several derived requirements that had to be considered during the design process. The following sections provide an explanation of how each of the derived requirements were extracted and why they were important to the design of the missile.

1. Propulsive Efficiency

The RFP dictates a threshold and objective range for the missile [1]. In order to accomplish these requirements, the missile must maximize propulsive efficiency, allowing it to meet or surpass both threshold and objective range requirements, as well as meet cruise requirements.

2. Lift, Vectored Thrust Production

In addition to specified range, the RFP also specifies cruise altitudes and speeds for both flight profiles and presents the objective of minimizing the launch-to-cruise transition distance [1]. These requirements imply that the missile must have the capability to produce enough lift and vectored thrust to achieve the specified values.

3. Propulsion Considerations for Cruise

From the given requirements for range and cruise, the missile will need a propulsion system that is capable of extended cruise segments. Thus, an air-breathing propulsion and a throttled solid rocket motor were analyzed as possible propulsion systems for the missile. Furthermore, the propulsion system must be analyzed to ensure its efficiency in the Mach ranges provided by the RFP [1].

4. Guidance, Navigation, and Control System

The RFP provides a trajectory following requirement and accuracy requirement (CEP). Each of these indicate that the missile will need to be equipped with an accurate guidance, navigation, and control system within the parameters specified. Additionally, the RFP provides altitude and speed ranges for both mission profiles. Since there are two profiles with distinct performance requirements and specified cruise altitudes, the missile will require a navigation system capable of executing predefined mission profiles. Lastly, the missile must be equipped with control authority in order to command high-g maneuvers, specified by the RFP, when necessary [1].

5. Structure Capable of Withstanding Loads

For the sea skimming mission profile, the RFP provides requirements for high-g maneuvers, including load factors and duration [1]. To ensure the missile can complete these maneuvers, its structure must be capable of withstanding the specified loads for the specified duration. This will be analyzed in the structural analysis, to determine the optimal structure material and thickness. A summary of the derived requirements is shown below in Table 3 [1].

Table 3. Derived requirements.

Requirement	Derived Requirements
<u>Range</u> Threshold: 60 nmi, Objective: 150 nmi	Maximize propulsive efficiency Produce enough lift/vectored thrust Propulsion system capable of extended cruise (air-breathing)
<u>Cruise Altitude</u> Maximum: 65,000 ft, Minimum: sea skimming	
<u>Launch-to-Cruise Transition</u> Minimize transition distance	Propulsion system that can quickly get missile to cruise speeds (booster)
<u>Trajectory Following</u> < 1500 ft of programmed	Accurate guidance, navigation, and control system
<u>CEP</u> 50 ft	
<u>High Diver Profile</u> Altitude: 5000 – 6500 ft, Speed: Mach 2.0 – 4.5	Navigation system capable of executing predefined mission profiles Air-breathing propulsion system efficient in these Mach ranges
<u>Sea Skimming Profile</u> Altitude: 15 – 200 ft, Speed: Mach 2.0 – 3.5	
<u>Maneuvers</u> Lateral Turns: 15 g, Vertical Turns: 7 g Duration: 45 s	Structure capable of withstanding necessary load factors Control authority to command high-g maneuvers

VIII. Approach

The following sections details the technical approach taken to develop the missile design environment. This includes the motivations behind the choice to use a design of experiments (DOE) to select the optimal missile design as well as the disciplinary analyses included in the missile analysis environment.

A. Motivation

Identifying an optimal missile design requires a synthesis of a series of sub-disciplinary analyses, such as aerodynamics, propulsion, and trajectory. However, traditional multidisciplinary optimization frameworks used for engineering problems are often ill-suited for missile design. Small changes in the design of the missile can have large, unpredictable effects on the overall missile performance, mostly caused by the trajectory analysis which contains an optimal control problem. Placing the trajectory analysis within a traditional optimization framework results in nested optimization loops which can cause traditional multidisciplinary optimization techniques, often relying on gradient-based optimization, to fail. Because of this, the process of identifying an optimal missile design cannot include an optimization loop.

To avoid a nested optimization loop, the optimal missile design was selected through a series of design space samplings. A selection of potential missile designs was identified using a DOE, which was used to maximize the amount of information gained by each experiment while sampling the design space. The potential missile designs were run through the missile design environment, which determined the performance of the missile design. The results of all the missile designs were aggregated to select a final missile design. A full explanation of the steps taken during the design space exploration and its results are discussed in Section IX: Design of Experiments.

The missile design environment encompasses the full analysis of a singular missile design. The missile design environment is composed of seven disciplines: geometry, propulsion, weights and structures, aerodynamics, trajectory, reliability, and life cycle analysis. An N^2 diagram showing the flow of information between disciplines is shown below in Fig. 1. As discussed previously in Section VIII.A: Motivation, the missile design environment does not feature any feedback optimization between disciplines.

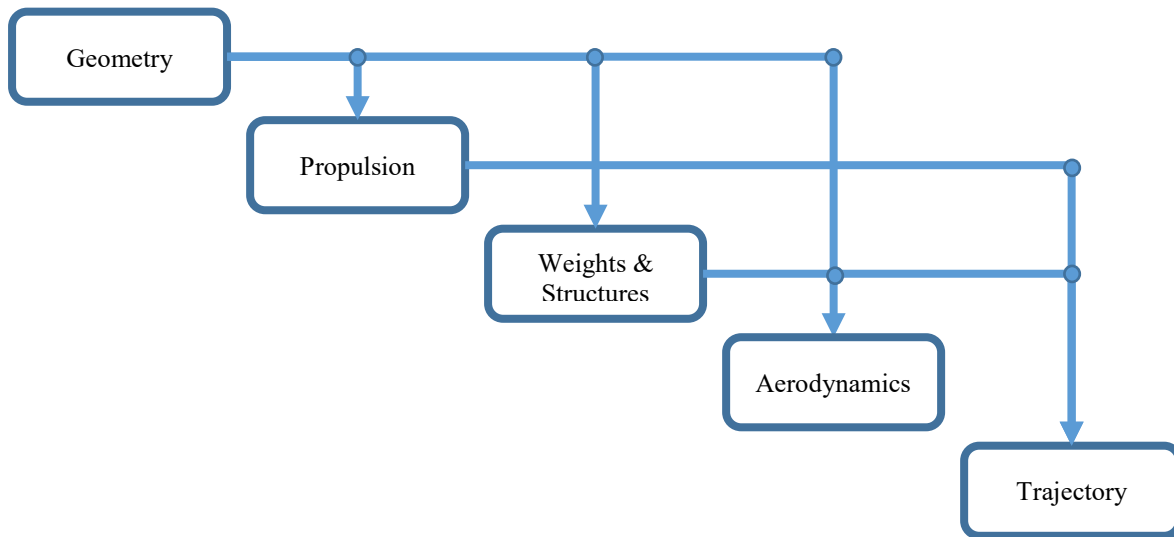


Fig. 1. Missile design environment N² diagram.

The inputs to the missile design environment are the features of a single missile design. Each individual disciplinary analysis determines both the performance of the design as well as its feasibility with respect to the given discipline. Because of the exploratory nature of a design of experiments and the way the missile was parameterized, the design of a missile may be considered infeasible for several reasons, which will be further discussed in the following sections. The result of the missile design environment is the cumulative performance of the missile from all the disciplines as well as the feasibility of the design. The entire design is considered infeasible if any individual discipline determines that the design is infeasible.

B. Geometry

Geometry serves as the starting point for the missile design environment. The geometry of the missile follows conventional cruise missile design guidelines. The external geometry of the missile is modeled as the buildup of six main components: nose, main body, inlets, wing, tail, and solid booster. The geometry takes in the variables from the DOE and converts them into the necessary geometric properties for the other disciplines in the missile design environment. The missile design environment can model a wide range of missile shapes. Several sample missile configurations are shown below in Fig. 2.

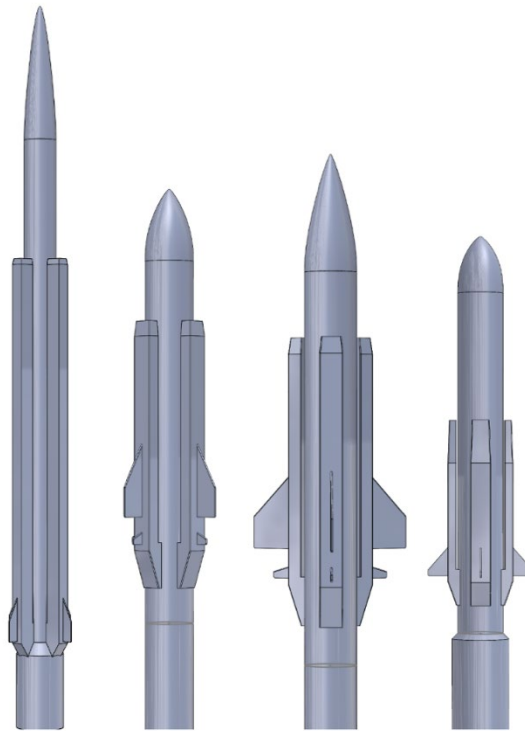


Fig. 2. Sample geometric missile layouts.

1. External Geometry

The overall length of the missile from the nose to the nozzle of the ramjet, not including any length added by a booster configuration, is defined by the missile length. The length of the missile is the largest driving factor of its overall size and performance. Large changes in the length of the missile have substantial impact on what would be considered an appropriate value or range for a several other parameters, such as the diameter of the missile or the location of the wing relative to the nose. As such, multiple parameters can be sized as ratios relative to the overall length of the missile. For example, instead of running over a range of missile diameters, the DOE can run over a range of missile fineness ratios, which is the ratio between the length of the missile and the missile diameter. This ensures the geometric feature is always an appropriate value for the given missile length so long as the ranges of possible ratios are appropriate. The size and shape of the nose are defined by the nose fineness ratio and the nose geometric shape.

The number of inlets, wing panels, and tail panels are together defined by a single parameter, the inlet-tail-wing configuration, in order to ensure rotational symmetry. The wings and tails are located on top of the inlets to maximize

available control moment. As the wing panels and tail panels are located on top of the inlets, the number of wing panels or tail panels must be factors of the number of inlets. This limits the number of compatible combinations, creating the necessity for a single parameter to define them all.

The wing and the tail geometries are defined by similar sets of parameters. The size and location of the wings and tails are defined by the total panel area and the trailing edge locations. The total wing or tail panel area is the sum of the areas of all the wing or tail panels, so a missile configuration with three wing panels will have larger individual panels than a missile configuration with four wing panels with the same total wing area. The wing or tail trailing edge location ratio is the location of the trailing edge of the wing or tail relative to the total missile length. The location of the wing or tail are defined by the trailing edge location to ensure the trailing edge of the tail does not hang over the end of the missile. The shape of the wings and tails are defined by the panel aspect ratio, the taper ratio, the trailing edge sweep, and the airfoil shape. Trailing edge sweep was selected instead of the more conventional leading-edge sweep due to the observation that supersonic missiles tended to have a wide range of leading-edge sweeps but a smaller range of trailing edge sweeps.

The inlets are modeled as 2D ramp inlets located axisymmetrically around the body. The size of the inlet is defined by the total inlet area, the inlet aspect ratio, and the inlet length ratio. The total inlet area is the sum of the frontal area of all the inlets. The inlet aspect ratio is the ratio between the height of an individual inlet and the width of an individual inlet. The inlet length ratio is the position of the start of the inlet as a ratio of the total missile length. From this point, the inlet goes down the length of the missile, all the way to the end of the missile before the solid booster. Additional shape parameters for the inlets include the angle of the inlet ramp and the height and length ratio of the diverter. Nose inlets were considered as valid configurations, but were incompatible with Missile Datcom, the code used for aerodynamic analysis.

The external shape of the solid booster is defined by its length, diameter, and position. Both the length and diameter of the solid booster are defined as ratios of the total missile length and the missile diameter, respectively. Additionally, the location of the booster depends on whether it is an aft drop-off booster or an integral rocket-ramjet. An integral rocket-ramjet must be able to fit within the ramjet of the missile, restricting the possible ranges of stage lengths and diameters. A full explanation on the selection of booster configuration and other internal booster geometry parameters is discussed in Section VIII.C.2: Boost Phase.

While the missile environment can simulate a wide range of geometric configurations, the exploratory nature of the DOE requires a limit on the number of parameters being varied to obtain reliable results, therefore, several geometric parameters had to be set to default values. These default values were obtained through researching similar performing supersonic missiles. The defaulted geometric parameters are shown below in Table 4.

Table 4. Defaulted geometric parameters.

Parameter	Default
Missile Ellipticity	1
Nose Shape	Ogive
Wing / Tail Aspect Ratio	1
Wing / Tail Taper Ratio	0.3
Wing / Tail Trailing Edge Sweep	0°
Wing / Tail Airfoil Shape	Hex
Inlet Location Ratio	40%
Inlet Aspect Ratio	1
Inlet Ramp Angle	20°
Diverter Height	0.02 ft
Diverter Length Ratio	2%

2. Internal Geometry

The internal packing of the missile was determined through a volume-based analysis. This was completed by comparing the sum of component volumes to the overall internal volume of the missile without the booster, based on its diameter and length. The volume of the nose is reserved for a warhead simulant ballast. Located behind the nose and the warhead simulant is the missile avionics bay, which is approximated to have a length of 3 ft based on a survey of similar systems. Following the avionics bay is the payload bay, which has a required length of at least 3.5 ft according to the RFP [1]. The rear of the missile will house the ramjet engine. There were no physical ramjet sizing tools available, so a length of 6 ft was selected based on a survey of similar systems. The remaining volume of the missile was allocated to the liquid fuel tank, which is located between the payload bay and the ramjet. A visualization of the internal packing of a sample missile design is shown below in Fig. 3.

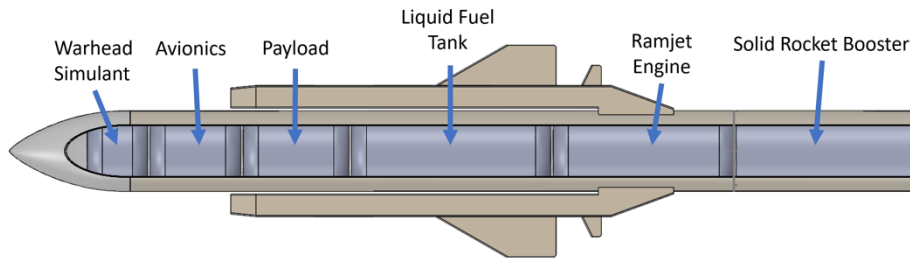


Fig. 3. Sample internal packing of missile.

Because of the flexible nature of the input space to geometry, some inputs will result in an infeasible design. For example, the use of missile length and missile fineness ratio to define the missile diameter can result in a missile design that does not meet the RFP’s minimum payload diameter of 10 in [1]. Additionally, if the total available volume for the liquid fuel tank is negative, which occurs when the length of the missile minus the length of the nose is less than 12.5 ft, the missile is also considered infeasible.

C. Propulsion

To begin the propulsion analysis, various types of propulsion systems were considered. This section will cover the process of narrowing down the propulsion systems to the liquid ramjet with a solid rocket motor booster. It will also describe how the two systems will be modeled as well as what considerations and theory were needed.

1. Air-Breathing Propulsion

Because the RFP requires a cruise segment for each of the flight profiles, an exploration of various types of air-breathing propulsion was performed. A turbofan and scramjet engine were immediately eliminated from the possible propulsion systems due to the flight profile speed requirements of Mach 2.0 to Mach 3.5/Mach 4.5. Thus, the analysis mainly focused on exploring the use of a ramjet versus a ducted rocket since both of these systems are efficient within these Mach ranges [11].

A ducted rocket, essentially a hybrid of a rocket and a ramjet, was initially considered due to having a higher thrust than ramjets and a higher specific impulse than solid propellant rockets [11]. However, the ducts themselves can be complicated and its Technology Readiness Level (TRL) was not high enough to consider it as a viable propulsion

system for an aerial target, as both of these factors translate to an increase in overall cost. Since there are no missiles that currently use ducted rockets, choosing this system was not a justifiable choice.

Besides being one of the least complicated propulsion systems as far as moving parts, ramjets are used on many missiles today. Its high TRL level, efficiency within the Mach ranges specified by the RFP, and ability to be throttled for cruise made the ramjet the optimal air-breathing propulsion choice for the ASDL-1776 [11].

Both solid and liquid fuels were considered for the ramjet, but solid propellant was ultimately discarded due to safety reasons. Using liquid fuel allows the engine to easily be throttled, stopped, and restarted. A liquid-fueled ramjet can be tested before operation, and most liquid propellants have nontoxic exhaust. The use of liquid fuel also allows the rocket to be fueled up before launch, meaning it is not as susceptible to accidentally exploding if dropped or hit compared to a rocket stored with solid fuel [12].

Numerical Propulsion System Simulation (NPSS) version 1.6.5 was initially used to model the ramjet. The NPSS block diagram, shown in Fig. 4, included elements AmbientNASA, InletStart, Inlet, DuctNASA, Burner, FuelStart, Nozzle, FlowEnd, and EngPerf. A simple solver was also used to calculate the temperature after the burner based on inlet air flow rate.

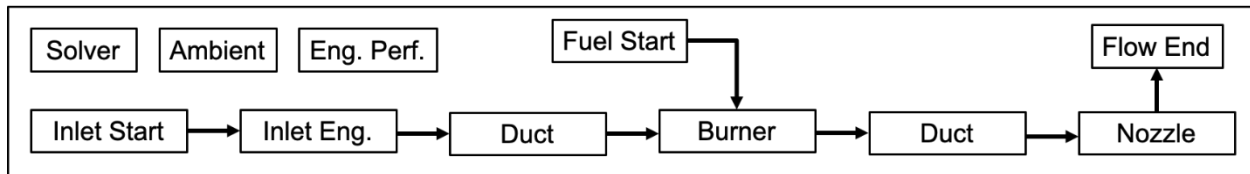


Fig. 4. NPSS ramjet block diagram.

The NPSS model was to run the ramjet through altitudes ranging from 0 ft to 65,000 ft and Mach numbers from 2.0 to 4.5. It would take in the inlet area from geometry and keep that as a constant, solving for the air mass flow rate and fuel mass flow rate. Each variation in inlet area would come from the DOE, representing a different vehicle.

The limiting factor on a turbojet or turboprop is the temperature before the turbine, due to the turbine materials. On a ramjet, this temperature limitation is not present. The limiting factor for ramjets comes from the inlet, specifically the pressure loss across the shock waves. A ramjet engine relies on slowing down the air flow to subsonic speeds before the burner, using a normal shock to accomplish this task. However, the pressure losses across a normal shock are great, thus, in order to minimize these losses, many ramjet inlets are designed to create multiple oblique shocks

before the terminal normal shock, increasing the pressure recovery and the range of Mach numbers for which the ramjet can function efficiently [13].

In order to properly model the ramjet inlet pressure recovery within NPSS, both Mil. Specs and shock tables were used and compared. The shock waves were accounted for using the equations shown below in Eq. (1), (2), and (3) [14], where γ is the specific heat ratio and α specifies whether the shock is a strong or weak shock solution. λ and X are placeholder variables. The shock angle, θ_{shock} , was calculated based on the Mach number ahead of the shock, M_1 , and the turning angle, δ . The weak shock solution was selected to minimize pressure losses when slowing down the flow. This allows for multiple oblique shocks followed by a single normal shock.

$$\tan(\theta_{shock}) = \frac{M_1^2 - 1 + 2\lambda \cos\left(\frac{4\pi\alpha + \cos^{-1}X}{3}\right)}{3\left(1 + \frac{\gamma-1}{2}M_1^2\right)\tan\delta} \quad (1)$$

$$\lambda = \left[(M_1^2 - 1)^2 - 3\left(1 + \frac{\gamma-1}{2}M_1^2\right)\left(1 + \frac{\gamma+1}{2}M_1^2\right)\tan^2\delta \right]^{1/2} \quad (2)$$

$$X = \frac{1}{\lambda} \left[(M_1^2 - 1)^3 - 9\left(1 + \frac{\gamma-1}{2}M_1^2\right)\left(1 + \frac{\gamma-1}{2}M_1^2 + \frac{\gamma+1}{2}M_1^4\right) \right] \tan^2\delta \quad (3)$$

$$\alpha = \begin{cases} 0 & \text{strong shock solution} \\ 1 & \text{weak shock solution} \end{cases}$$

The Mil. Spec used for the NPSS model was MIL-E-5007D. It was found that the calculations based on shock tables, which included multiple oblique shocks followed by a normal shock, gave a lower estimate of overall pressure recovery than the Mil. Spec. Also, the Mil. Spec did not account for the temperature variation across the shocks. NPSS automatically calculates a temperature rise between the ambient element and the burner, but this rise was found to be greater than what was calculated using the shock tables. It was decided to use the shock tables instead of the Mil. Spec, since this would give more accurate results with respect to both the pressure and temperature variations across the inlet.

The NPSS model was to run the ramjet through altitudes ranging from 0 ft to 65,000 ft and Mach numbers from 2.0 to 4.5. It would take in the inlet area from geometry and keep that as a constant, solving for the air mass flow rate and fuel mass flow rate. Each variation in inlet area would come from the DOE, representing a different vehicle. After building the model, it was found that the inlet area would continually change with respect to the inlet air mass flow rate, making use of the DOE variables meaningless. Also, the output for the code gave fuel mass flow rates and

calculated inlet areas that were physically impossible. It is believed that the difficulty of changing a variable designated as an output in NPSS to an input, paired with the need for a compressor and turbine element in most NPSS calculations, led to these inconsistencies. Because the difficulties encountered with using NPSS could not be rectified in a timely manner, it was decided that the specific impulse of the ramjet would be used instead, based upon information given from Fleeman, shown in Fig. 5 [11].

Specific impulse (I_{SP}) of the ramjet was estimated using Equation (4), where M_0 is the Mach number, H_f is the heating value of fuel, T is the combustion temperature ratio, a_0 is the speed of sound, and γ is the specific heat ratio. The estimation was based off an ideal ramjet baseline with a combustion temperature optimized for Mach 3.5 and finds I_{SP} as a function of current Mach number. Equation was derived by creating a polynomial fit for the I_{SP} of a known ramjet baseline, shown in Fig. 5 [11].

$$I_{sp} = \frac{H_f}{a_0} \left(\frac{(\gamma - 1)M_0}{1 + \frac{\gamma - 1}{2} M_0^2} \right) \left(\frac{T}{1 + \frac{\gamma - 1}{2} M_0^2} \right)^{1/2} + 1 \quad (4)$$

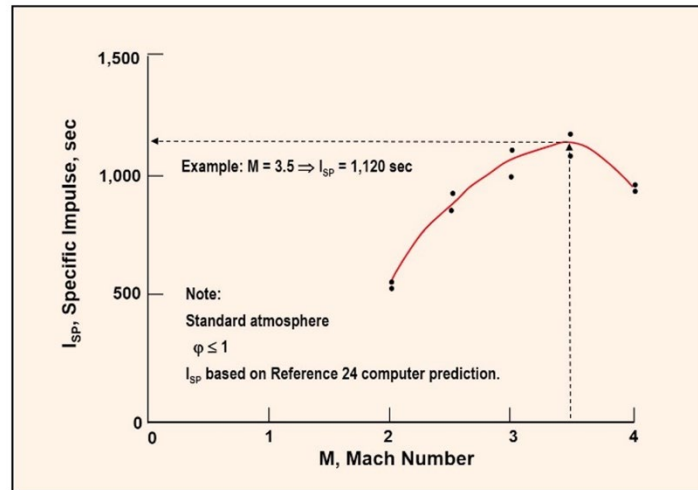


Fig. 5. Specific impulse modeling of ramjet.

The I_{SP} model assumes isentropic flow, perfect gas, and ideal expansion. It also assumes a combustor with sufficient length to allow for complete combustion, which is a reasonable assumption for altitudes below 60,000 ft. Due to these assumptions, the estimated I_{SP} is likely to be slightly higher than reality.

2. Boost Phase

Because a ramjet was selected for optimum missile performance, a means of achieving the necessary speed for optimum ramjet performance was necessary. A ramjet engine starts being efficient at around Mach 2.0 [11]. A booster stage is necessary to achieve this speed for the ram effect to generate enough compression for optimum engine efficiency.

There is no commercially available solid rocket motor code that would be able to size the booster stage. To properly model the boost stage of the ASDL-1776 missile, an algorithm had to be developed to determine the necessary outputs which include Mach No., mass flow rate, mass flux rate, chamber pressure, optimum grain geometry, and propellant mass. The current code developed by Casey Wilson [15] had some of the necessary capabilities but needed to be rewritten and modified to handle the DOE and the most effective solid rocket motor (SRM) grain and geometry design. The grain varying capabilities of the code were imperative so that the DOE would select the lowest cost and most effective solid rocket motor. What follows is a description of the grain geometry capabilities of the code as well as an explanation on how the burn simulation operates.

The code itself can be broken down to two main modules. The first module generates the geometric output of an arbitrary geometry using an internal and external edge finding algorithm. The second module inputs the geometric output and simulates the burn of the solid rocket motor via an unsteady model. Fig. 6 shows a visualization of the geometric burn algorithm. The blue line represents the original propellant core boundary while the red circles represent the growing circular boundary of propellant consumption at a given time step [15].

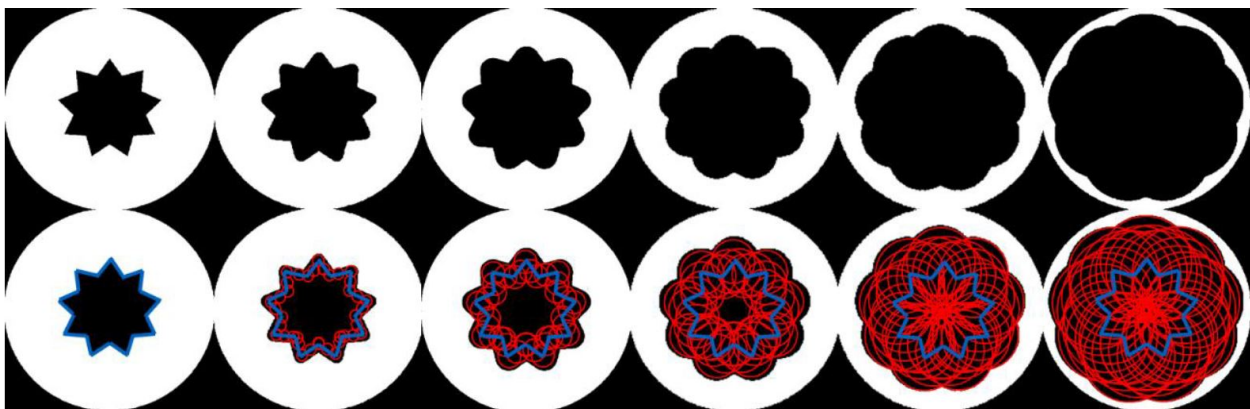


Fig. 6. Visualization of geometric burn algorithm.

Grain geometry variation is a key input factor that influences the solid rocket motors performance and was a factor that varied in the final DOE. The grain capabilities were expanded to include four unique geometries, shown in Fig. 7 [15].

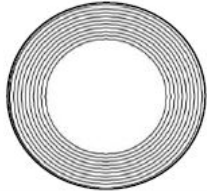
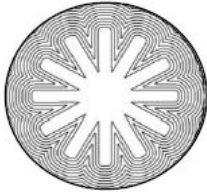
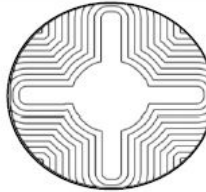
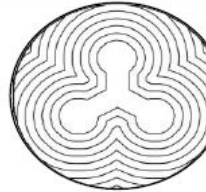
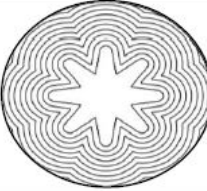

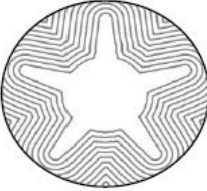
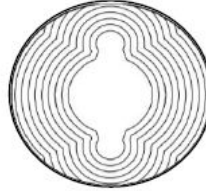
Grain Type	Example 1	Example 2	Example 3
<i>BATES</i>			
<i>Finocyl</i>			
<i>Star</i>			
<i>Starocyl</i>			

Fig. 7. Core geometries handled by SMAC 3.1.

One of the most important varying parameters in the DOE was the grain geometry since it significantly impacts the thrust profile and SRM performance. A properly selected grain geometry minimizes the cost and performance of the missile. The four different grains can be divided into geometries with fins (Finocyl, Star, Starocyl) and grain geometries without fins (BATES). Fins increase the initial area exposed to the oxidizer which creates a regressive thrust profile. This is beneficial for the missile design because it enables vehicle liftoff. Finned geometries also introduce important variables that were explored in the DOE for example fin width, fin number, inner grain diameter, port diameter, and dumbbell size. A BATES geometry allows for a greater amount of propellant which translates to higher total thrust. Due to the different benefits of the four different geometries it was imperative to explore this variable in the DOE.

3. *Propellant Section*

For the booster stage, several different propellants from the available literature were considered. Unfortunately, the publicly available data on propellant specific values was sparse so the down selection of the propellant was simple. A choice of AL + HTPB was selected based on the solid propellant's efficiency and cost [11].

D. Weights & Structures

For the weights and structures analysis, the overall missile weight and center of gravity at various points in the mission must be calculated. The center of gravity location impacts missile stability, so it is critical to ensure that as the missile burns fuel throughout the mission it remains in a stable configuration. A stress analysis of the missile body was also completed to demonstrate ASDL-1776's ability to meet the requirement for high g maneuvers without compromising its structural integrity.

1. *Weights and Center of Gravity*

Missile weight and center of gravity (CG) locations affect stability and various flight performance requirements, including speed, range, and maneuverability. Weight and center of gravity location will be estimated by developing parametric equations using defined quantities such as wing size, booster size, airframe material, and component locations along the missile center axis, as well as known or estimated material densities. These equations will be contained in a custom MATLAB script that runs through each defined vehicle in the given DOE and will output a weight and center of gravity distance from nose at four flight conditions: launch, solid booster burnout, solid booster drop, and liquid fuel depletion. Each of these outputs will assume a full payload of 500 lbs. for initial sizing as specified by the RFP [1]. The assumptions and calculations used to determine the weight of each component are shown below in Table 5. The densities for the weight estimates are obtained from Fleeman [11].

The total launch weight of the vehicle W_{launch} is calculated as the sum of the weights of each of the components listed below in Table 5. The weights at the critical flight conditions can be calculated as shown below in Eq. (5), (6), and (7).

Table 5. Component weight estimation.

Component/Subsystem	Volume (ft ³)	Density (lb/ft ³)	Weight (lbs.)
Warhead	5	120.96	604.8
Avionics	$3\pi d^2/4$	69.12	Volume * Density
Payload	-	-	500
Aerodynamic Surfaces	Defined in DOE	466.56	Volume * Density
Liquid Fuel Reservoir	Remaining unused volume	103.68	Volume * Density
Ramjet	$6\pi d^2/4$	466.56	Volume * Density
Ramjet Casing	Output from Stress script	466.56	Volume * Density
Empty Structure	Output from Stress script	172.8	Volume * Density
Solid Booster Casing	Defined in DOE	466.56	Volume * Density
Solid Booster Propellant	-	-	Output from SRM code

$$W_{burnout} = W_{launch} - W_{propellant} \quad (5)$$

$$W_{drop} = W_{burnout} - W_{booster} \quad (6)$$

$$W_{depletion} = W_{drop} - W_{fuel} \quad (7)$$

$W_{burnout}$ represents total weight at solid rocket booster burnout, W_{drop} is total weight after the booster is dropped, and $W_{depletion}$ is total weight after liquid fuel depletion. $W_{propellant}$ is the weight of the solid rocket booster propellant, $W_{booster}$ is the weight of the solid rocket booster casing, and W_{fuel} is the liquid fuel weight.

The weights defined by Table 5 are then paired with a component location to calculate center of gravity location at each of the four flight conditions. The component locations are defined based on the packing assumptions discussed in Geometry. All components are assumed to have an even weight distribution, and therefore their location is defined as their midpoint. Then the center of gravity location at launch, $x_{CG,launch}$, can be calculated in ft from nose as shown in Eq. (8).

$$x_{CG,launch} = \frac{\sum(W_1x_1 + W_2x_2 + \dots)}{W_{launch}} \quad (8)$$

W_1, W_2, \dots refer to component weights from Table 5, and x_1, x_2, \dots refer to respective component locations. The missile is assumed to be radially symmetric, and therefore center of gravity is only calculated in the longitudinal direction. The location of the center of gravity at other flight conditions are calculated as shown below in Eq. (9), (10), and (11).

$$x_{CG, burnout} = \frac{x_{CG, launch} W_{launch} - x_{booster} W_{propellant}}{W_{burnout}} \quad (9)$$

$$x_{CG, burnout} = \frac{x_{CG, launch} W_{launch} - x_{booster} W_{propellant}}{W_{burnout}} \quad (10)$$

$$x_{CG, drop} = \frac{x_{CG, burnout} W_{burnout} - x_{booster} W_{booster}}{W_{drop}} \quad (11)$$

In these equations, $x_{CG, burnout}$ is CG location at solid rocket booster burnout, $x_{CG, drop}$ is CG location after the booster is dropped, and $x_{CG, depletion}$ is CG location after liquid fuel depletion. $x_{booster}$ is the distance of the solid rocket booster from the nose, and x_{fuel} is the distance of the liquid fuel reservoir from the nose. The script will also simulate a varying payload for any given design to show the variation of CG location with payload weight at each of the four mission conditions.

2. Structural Analysis

A structural analysis was necessary in order to determine whether the body of the missile would be capable of withstanding forces throughout each of the flight profiles defined in the RFP [1]. To analyze the forces felt on the missile throughout the mission, hoop stress, bending, and buckling of the missile body will be considered. The missile body will also experience some longitudinal stress, but this is typically smaller than the hoop stress and therefore can be ignored.

The analysis was based on the Georgia Tech 2014 entry to the AIAA MSTC competition [16]. The module calculates the required skin thickness for every separate stage of the missile based on the geometry of the missile, component weights, expected mass thrust and drag, chamber pressure of ramjet and solid rocket booster, and maneuver loads. The loads were combined to find the principal stresses acting on the body, and a factor of safety (FOS) is derived from the material properties. The module begins with a skin thickness of 0.1 in. and then determines the FOS for each stage. If all stages do not meet the minimum FOS, it then incrementally increases the thickness by 0.001 in. individually for each stage and reevaluates after every iteration until all stages meet the desired FOS.

The missile was divided into three stages based on their expected loads in order to simplify calculations. The first stage extended from the nose of the missile to the beginning of the ramjet chamber. The second stage was defined as the structure around the ramjet combustion chamber. The third stage was defined as the structure around the solid rocket booster.

The monocoque structure of the missile allows for a physics-based analysis due to it being a single continuous part, its ability to be modeled with basic structures, and its lack of complex linkages that would be difficult to model without advanced finite element analysis. In order to accurately estimate a required skin thickness, several assumptions about the flight loads and structure of the missile needed to be made.

The missile was assumed to be constructed of three concentric thin hollow cylinders corresponding to each of the three stages. The cylinders were assumed to be fixed to each other and that their linkage was significantly stronger than the cylinders themselves, so that any point of failure would occur on the cylinders themselves rather than the connection point. All cylinders were also assumed to be homogeneous and isotropic.

All openings in the structure for actuators and other external features were assumed to have an insignificant impact on the strength of the structure and would be accounted for in the factor of safety. An FOS of 1.5 was selected based on a historical precedent for motor casings as described in Ref. [11]. The mass of the missile subsystems was assumed to be evenly distributed throughout the internal volume of the missile.

The last assumption was that every load was evaluated at its maximum case simultaneously in order to obtain the absolute maximum stress that can be incurred on the structure. Although this evaluation would not occur or be possible in a normal flight, estimating at the maximum adds an additional degree of redundancy and ensures the structure would survive all complex load cases. The total stress is therefore calculated at simultaneous maximum thrust, maximum drag, and while performing terminal maneuvers.

3. Material Selection

Several materials were selected to create the body of the missile. The first stage was composed of Aluminum 2024-T3 due to its strength and relatively low weight compared to other common aluminum and steel alloys [17]. Additionally, its extensive and common use in aerospace ensures lower development costs as its characteristics and machinability have been well explored. It has shown suitable qualities in similar missiles such as the Standard Missile-2 ER and survivability at speeds of up to Mach 4.5 [18].

The second and third stages involve significantly higher stresses and temperatures due to their proximity to the ramjet and booster, respectively. Due to this, Steel 4340 was selected because of its higher service temperature and relatively high yield strength [17]. Steel allows for thinner skin and thinner insulation, providing more room for the components inside and reducing complexity in exchange for slightly higher weight. The ramjet combustion chamber is lined with a coating of flame-sprayed zirconium dioxide which provides protection from the high temperatures created by the ramjet and resistance to oxidation [19].

The missile cone was constructed out of Pyroceram 9606 due to its high service temperature and common use in similar missiles leading to lower development costs [17]. The Pyroceram radon's design can be modified to work a variety of electronic signals making ASDL-1776 more versatile in its ability to mimic numerous threats.

More advanced materials such as composites or superalloys were not considered, as their additional development and production costs would not provide significant advantages to the use of ASDL-1776 as a training missile.

1. Factor of Safety Calculation

Bending loads due to maneuvers were estimated using a nomogram outlined by Ref. [11] as a function of applied g-force, length and type of loading. The applied g-force was determined to be 15 g's as specified by the RFP [1]. The bending moment generated during these maneuvers M_b can be calculated as a function of the mass m , acceleration due to gravity g , the maneuver load factor n , the length of the missile with the booster dropped L , and the loading condition c , as shown below in Eq. (12).

$$M_b = \frac{mgL}{c} \quad (12)$$

Maneuver loads were estimated as a rear biased linear load ($c = 7.8$) due to position of the fin sets [11]. The maximum stress due to this load is then calculated as a function of this bending moment M_b , the body radius r , and the thickness of the frame t , as shown below in Eq. (13).

$$\sigma_B = M_b \frac{1}{\pi R^2 t} \quad (13)$$

No ejection loads were estimated since the missile surface launched, and all handling loads were assumed to be less than the maneuver loads.

Hoop stresses were considered in order to ensure the structural integrity of the second and third stages. The module evaluated if the structure would be able to match the desired factor of safety at the maximum pressure created from the ramjet and solid rocket motor (SRM) during operation. It was assumed that the only contribution to hoop stress was from these pressures. The stress due to these internal pressures σ_h was calculated as a function of the chamber pressure P_c , the inner radius R , the skin thickness t , and the length of the stage L as shown below in Eq. (14).

$$\sigma_h = \frac{\pi P_c R}{t} \quad (14)$$

Dome stress was not considered in the module as it was assumed to be part of the combustion chamber casing, meaning its weight is accounted for in the ramjet engine weight estimation rather than the missile skin and structure.

The last failure mode approximated by the design environment is buckling due to applied axial loads. The force applied is assumed to be the sum of the maximum drag, maximum weight, and maximum thrust that can be experienced by the missile. The stress induced σ_A is calculated as a function of the applied force F_c and the cross-sectional area of the stage A_{cr} as shown below in Eq. (15).

$$\sigma_A = \frac{F_c}{A_{cr}} \quad (15)$$

E. Aerodynamics

The aerodynamics of the missile were computed using Missile Datcom, a semi-empirical data compendium software for predicting missile aerodynamics for preliminary design and analysis. Missile Datcom was developed by the United States Air Force and is restricted under International Traffic in Arms Regulations (ITAR).

The inputs to Missile Datcom are the geometric properties of the missile, the flight conditions to simulate, and the program execution settings. Missile Datcom uses a component build-up method to define the geometry of the missile. The geometric properties of the missile include both the shape of the missile from geometry as well as the center of gravity from weights and structures. Runs were made with both the booster attached and detached to model aerodynamics throughout all phases of flight. Missile Datcom was run over a range of angles of attack from -35° to 35° , altitudes from 0 feet to 65,000 feet, and Mach numbers from 0.01 to 4.5.

For each flight condition, the lift coefficient (C_L), the drag coefficient (C_D), and the pitching moment coefficient derivative with angle of attack ($C_{m\alpha}$) are recorded. The C_L and C_D results are combined with the angle of attack,

altitude, and Mach number into a series of data look-up tables used by the trajectory optimization. Visualizations of the C_L and C_D data tables generated for a sample missile geometry are shown below in Fig. 8.

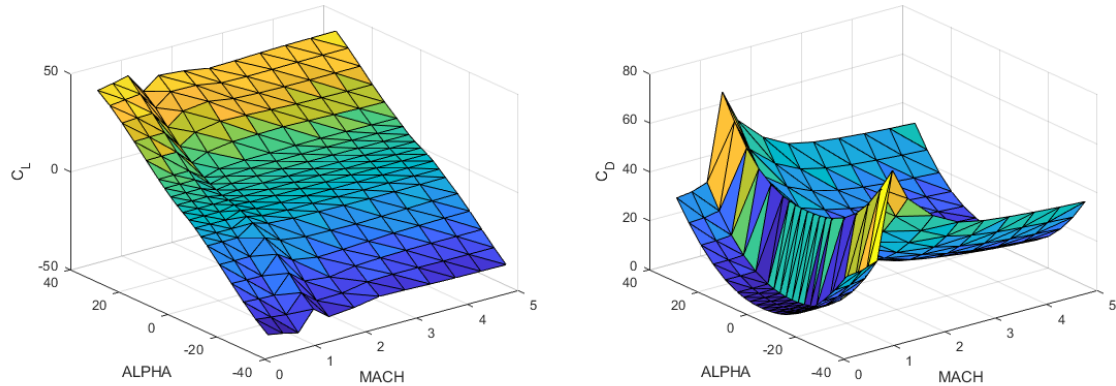


Fig. 8. Lift coefficient (C_L) and drag coefficient (C_D) surfaces generated by Missile Datcom.

The $C_{m\alpha}$ results are used to determine the stability of the missile. The static stability criteria require that the missile have an initial tendency to return to initial conditions after a disturbance. This is primarily a concern in the longitudinal plane, involving disturbances in the angle of attack or pitch of the missile. The longitudinal static stability criterion is that $C_{m\alpha}$ must be less than zero, meaning that a positive change in angle of attack results in a negative pitching moment and vice versa. As $C_{m\alpha}$ varies throughout the different flight conditions, it was decided that any vehicle that encounters a $C_{m\alpha} > 0$ at any flight condition would be considered infeasible. While advanced flight control systems could allow a missile to operate with longitudinal static instability, the current criterion was deemed acceptable. A visualization of the changes in $C_{m\alpha}$ for a sample missile geometry are shown below in Fig. 9.

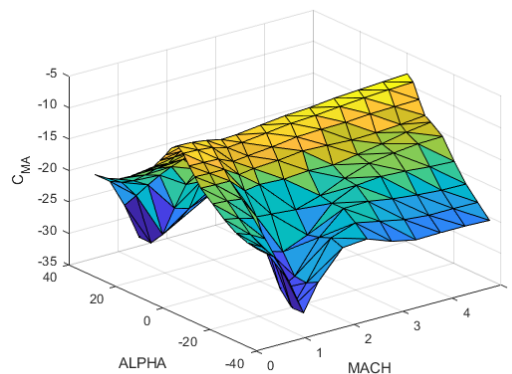


Fig. 9. Pitching moment coefficient derivative with angle of attack ($C_{m\alpha}$)

F. Trajectory

The trajectory analysis will provide a method to determine if a missile architecture satisfies the mission requirements laid out in Table 2. The equations of motion require the models for aerodynamic forces, the thrust and mass flow of the propulsion systems and the initial weight from the weights and structures model.

1. Equations of Motion

Performing trajectory analysis requires selecting a set of equations of motion to model the kinematics of the missile. The propose of the trajectory analysis is primarily as a method for determining the potential performance of the given missile design. Selecting an optimal control design is not a part of that objective. Therefore, point-mass equation of motions will be used to model the missile as opposed to modeling roll, pitch, and yaw rates. Because the requirements only have a down-range requirement, the analysis can be simplified to a 2-D system with motion restricted to motion in the vertical plane. Had there been a cross-range requirement, the motion in the horizontal plane would have been considered as well. The missile will have a short flight as the range threshold is 60 nmi and the objective range is 150 nmi. Because of this, a flat, non-rotating earth system can be used.

The first set of equations of motion are the time derivatives of velocity, or acceleration, of the vehicle, split into the x-axis \dot{V}_x and the z-axis \dot{V}_z . The x-axis and the z-axis refer to the range and altitude of the missile, respectively. These are a function of the mass of the vehicle m and the four primary forces experienced by the missile: lift L , drag D , thrust T , and weight W . The accelerations are calculated as shown below in Eq. (16) and (17).

$$\dot{V}_x = \frac{T * \cos(\theta) - \frac{1}{2}\rho V^2 S C_D \cos(\gamma) - \frac{1}{2}\rho V^2 S C_L \sin(\gamma)}{m} \quad (16)$$

$$\dot{V}_z = \frac{T * \sin(\theta) - \frac{1}{2}\rho V^2 S C_D \sin(\gamma) + \frac{1}{2}\rho V^2 S C_L \cos(\gamma) - W}{m} \quad (17)$$

The second set of equations of motion are the time derivatives of position, or velocity, of the vehicle, split into the x-axis \dot{s} and the z-axis \dot{h} . They are a function of the velocity of the missile V , which is numerically integrated from Eq. (16) and (17), and the flight path angle γ , as shown below in Eq. (18) and (19).

$$\dot{s} = V * \cos(\gamma) \quad (18)$$

$$\dot{h} = V * \sin(\gamma) \quad (19)$$

The final equation of motion is the time derivative of mass of the vehicle m . As the vehicle flies, it will lose mass both from burning fuel \dot{m}_{fuel} and from dropping the boosters $m_{booster}$. The loss of fuel occurs constantly through the flight process while the loss of weight from the booster occurs instantaneous after the boost phase. The equation to calculate the change in mass is shown below in Eq. (20).

$$\dot{m} = \dot{m}_{fuel} + \begin{cases} m_{booster} & \text{for SRM drop} \\ 0 & \text{else} \end{cases} \quad (20)$$

From the equations of motion, the trajectory was broken down into three flight segments, the boost phase, the cruise phase and then the dive or terminal phase. The boost phase was defined from launch to the solid rocket motor burnout, with the objective to accelerate the missile to at least Mach 2 for the ramjet. After the rocket motor burned out and the case dropped, the ramjet would ignite to start the cruise phase. The objective of the cruise phase was to maintain the designed Mach and altitude until either the objective range was met, or the liquid fuel was consumed. After either condition was met, the missile would enter the dive phase until ground impact, an altitude equal to zero.

2. Aerodynamics

The velocity and position were integrated through the equations of motion. To calculate the aerodynamic forces and Mach number, the 1959 ARDC Model Atmosphere model was used to determine the air density and speed of sound for a given flight altitude [20].

For all three stages, the aerodynamic coefficients for lift and drag are determined from Missile Datcom as discussed in Section VIII.E: Aerodynamics. The aerodynamic tables were defined and tested in Missile Datcom on a discrete interval as a function of the altitude, angle of attack, and Mach number. During the trajectory propagation, the coefficients at any altitude, angle of attack and Mach number were then calculated through the linear interpolation method of the data from nearest known points calculated in Missile Datcom. Two sets of data tables were required to model the full trajectory. During the boost phase, the aerodynamic coefficients are interpolated from the data table generated with a model of the booster attached to the main missile body. Then after the booster was dropped, during the cruise and dive phases, the aerodynamic coefficients were interpolated from a second table generated with model for the main missile body.

3. Propulsion

During the boost phase, the thrust and mass flow rate are interpolated from a solid rocket engine deck generated by the solid rocket engine code as a function of the burn time. After the boost phase, there will be a check to ensure the missile has achieved the required Mach number to allow for safe ignition of the ramjet engine for the cruise phase. For an aft drop-off booster, there is an additional change in mass to account for the mass of the rocket structure.

The thrust and mass flow rate for the cruise and dive phase were modeled using the ramjet specific impulse model described in Section VIII.C.1: Air-Breathing Propulsion. Under constant speed cruise conditions, the throttle setting would be set such that thrust equals drag. When the current speed is below the designed Mach number, the thrust required is solved for by using Eq. (21) below. From this equation, if the missile is flying below the design Mach number, the thrust required will be greater than drag to accelerate, so the throttle setting would increase. Whereas if the missile is flying faster than the designed Mach number, the throttle setting will decrease to decelerate. From the required thrust and the specific impulse, the ramjet propellant mass flow rate was calculated using Eq. (22). Once the liquid fuel has been consumed, the thrust and mass flow rate are both zero.

$$T = \frac{M_{des}}{M} * D(h, M, \alpha) \quad (21)$$

$$m_{fuel} = \frac{T}{I_{SP}(M, h) * g} \quad (22)$$

4. Trajectory Propagation

The trajectory code was developed using a direct shooting method to simulate the flight of the missile. For defining the trajectory, the RFP defines an allowable range for the flight attitude and speed but no strict requirement [1]. These two variables will act as flight path constraints for the trajectory propagation problem. The cruise phase of the trajectory is defined by a design altitude and Mach number. The flight path angle and angle of attack acted as the control variables at to be able to achieve the design altitude and Mach number between each time step of the integration. missile must achieve a 60 nmi down-range threshold requirement with a 150 nmi objective. Discretizing the trajectory into small segments, the range of each missile architecture was solved for by propagating the equations of motion.

5. Midcourse Terminal Approach

The analysis of a flight trajectory where the missile should enter the terminal phase immediately after reaching the cruise condition was also required. The trajectory was defined using a desired cruise speed and altitude. Once the cruise altitude was achieved, the trajectory propagation was stopped so the cruise phase immediately ended. Then the dive phase started with the objective of maximizing vertical velocity, creating a steepest decent flight profile with the constraint of a 75° maximum dive angle. At any point throughout the duration of the trajectory, the cruise phase could be terminated to allow the missile to enter the dive phase before achieving the maximum range. An example of this is where the maximum range is 182 nmi in Fig. 10, and then an early terminal phase was commanded at 50 nmi to hit a target at 52 nmi on impact as seen in Fig. 11.

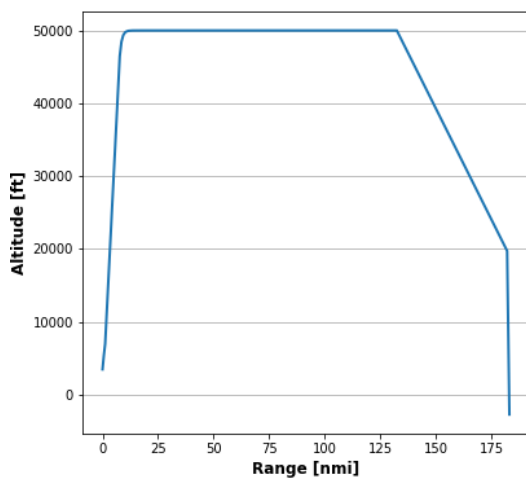


Fig. 10. Maximum range cruise trajectory.

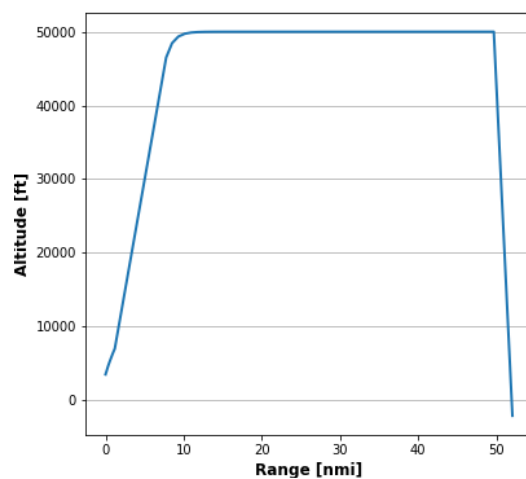


Fig. 11. Early terminal dive trajectory.

6. Circular Error Probable

ASDL-1776 will include a Guidance, Navigation, and Control System in order to program, guide, and control the missile trajectory. The FAA GPS Performance Analysis Report, available in Ref. [22], shows the average user range error accuracy to be less than 29.5 ft horizontal error and 49.2 ft vertical error, 95% of the time. Further, the measured performance exceeds those averages with less than 6.2 ft horizontal error and less than 12.7 ft vertical error. Thus, a standard Guidance, Navigation, and Control System should provide sufficient accuracy to meet the CEP requirement of 50 ft as well as the trajectory following requirement of ± 1500 ft as specified in the RFP [1].

G. Cost and Manufacturing Modeling

The total cost of producing each ASDL-1776 missile was estimated using a function of the weight derived from correlating data on similar tactical missiles in Ref. [11]. The function was modified to account for cost saving measures implemented in other phases of design. Using more common and less expensive alloys for the body structure was assumed to yield a 5% reduction in unit costs. Additionally, the Modular Avionics Control Hardware (MACH) system from the GQM-163A Coyote was chosen as the guidance and control system to further save on development costs. The MACH system is modular and the GQM-163A is capable of similar sea-skimming and high-altitude flight profiles, so it will be capable of meeting the requirements of the RFP [1]. This usage of the MACH system was assumed to yield additional 5% reduction in per unit costs. Eq. (23) was used to find the total cost per unit, where C_m is the cost in 2020 dollars and W_l is the weight in pounds.

$$C_m = \$8640 * W_l^{.64} \quad (23)$$

The cost of the entire production run was estimated based on the per unit cost with a logarithmic learning curve. Eq. (24) shows the cost estimate, where C_n is the cost of the n th unit produced, L is the learning curve constant, and n is the number of the unit produced. 90% was selected as the value for L since it is a typical value for production costs [11].

$$C_n = C_m L^{\log_2 n} \quad (24)$$

The total production cost is the sum of all individual units for the production run plus the cost of the launch platform. C is the total cost, N is the number of units in the production run and C_l is the cost of the chosen launch platform, as shown in Eq. (25).

$$C = C_l + \sum_{n=1}^N C_n \quad (25)$$

H. Maintenance and Safety Considerations

The role of ASDL-1776 as a target missile results in a unique operational and maintenance cycle compared to traditional missiles. A majority of ASDL-1776's service life will be spent in storage until a test is authorized and it is deployed. Storage will likely be in a controlled facility with a set temperature and humidity and little to no vibrations

or shocks. This allows it to remain in storage over extended periods of time without issues such as corrosion. The rocket will be stored with no liquid fuel to prevent accidental combustion or leakage and will be fueled prior to launch. The solid booster is capable of being stored for up to 10 years without issue, meeting the requirements of the RFP [1].

To ensure reliability, a Missile Subsystem Test Set (MSTS) test can be performed at yearly intervals or prior to launch to ensure functionality. Since quick deployment is not critical for a target missile, larger intervals between MSTS tests are practical to further reduce costs.

The modular payload of ASDL-1776 can be varied depending on the target it is intended to mimic. This payload can therefore be installed during initial construction if it is fixed, or just prior to deployment if it varies between launches.

IX. Design of Experiments

The following section details the approach taken to identify the final missile design. This process included a series of several DOEs used as ranging experiment to understand the effect of variable on the overall performance of the missile as well as reduce the design space to exclude infeasible designs. Once the design space was shrunk, a final DOE was run to generate a list of viable vehicles. A multi-attribute decision making method known as TOPSIS was used to identify a final design.

A. Body Sizing Ranging Experiment

The objective of the first ranging experiment was to obtain a general idea for the sizing of the missile body and the feasibility of various parameter combinations. To that end, several parameters identified as having significant effects on the missile performance and feasibility were selected for the ranging experiment. As there were no previous results to work from, the parameter ranges selected for the first ranging experiment are quite wide. While this may result in designs that are either infeasible, ill-suited for the missions at hand, or both, it provides an initial guess for developing more intelligent ranges for future experiment. The selected parameters and their ranges are shown below in Table 6. The parameters that were not selected for varying in the DOE had to be set to a default value. These values were rough estimates of appropriate values and would be further explored in later a later DOE. The defaulted parameters are shown below in Table 7. As the solid booster grain geometry was defaulted to Bates, which is a simple geometry, there were no values for several of the complicated solid motor geometry parameters.

Table 6. Variables and ranges for body sizing ranging experiment.

Parameter	Minimum	Maximum
Missile Length	10 ft	40 ft
Missile Fineness Ratio	5	20
Nose Fineness Ratio	2	5
Wing Total Area	5 ft ²	25 ft ²
Wing Trailing Edge Location Ratio	45%	80%
Tail Total Area	1 ft ²	5 ft ²
Tail Trailing Edge Location Ratio	80%	100%
Inlet Total Area	0.5 ft ²	3 ft ²
Solid Booster Stage Length Ratio	10%	40%
Solid Booster Grain Inner Diameter Ratio	10%	35%

Table 7. Variables and ranges for first design of experiments.

Parameter	Default
Inlet-Wing-Tail Configuration	4/4/4
Solid Booster Stage Diameter Ratio	100%
Solid Booster Grain Geometry	Bates
Solid Booster Grain Fins	-
Solid Booster Grain Port Diameter Ratio	-
Solid Booster Grain Dumbbell Diameter Ratio	-
Solid Rocket Grain Fin Width Ratio	-

A DOE containing 500 sample vehicles was created in JMP, a statistical analysis suite. The vehicles were distributed using Latin hypercube sampling, a space filling method useful for computer-based experiments. The vehicles were run through the missile design environment, but only through the high diver flight profile, not the sea skimming flight profile. The results were collected and the parameters from the design of experiments were compared against the results to identify trends and patterns.

The first result explored is whether the vehicles meets the payload diameter constraint. The payload bay must have a diameter of at least 10 inches, as discussed in Section VIII.B.2: Internal Geometry. Additionally, there also must be space for the structural skin surrounding the payload, as discussed in Section VIII.D.2: Structural Analysis. If the missile diameter is less than the sum of the structural skin thickness and the payload diameter constraint, then the

vehicles does not meet the constraint. Of the 500 vehicles ran, 446 met the payload diameter constraint, an 89.2% success rate. A constraint scatterplot matrix showing the vehicles that meet or break the payload diameter constraint, shown in black and gray respectively, plotted against the missile length, missile fineness, and resulting missile diameter is shown below in Fig. 12.

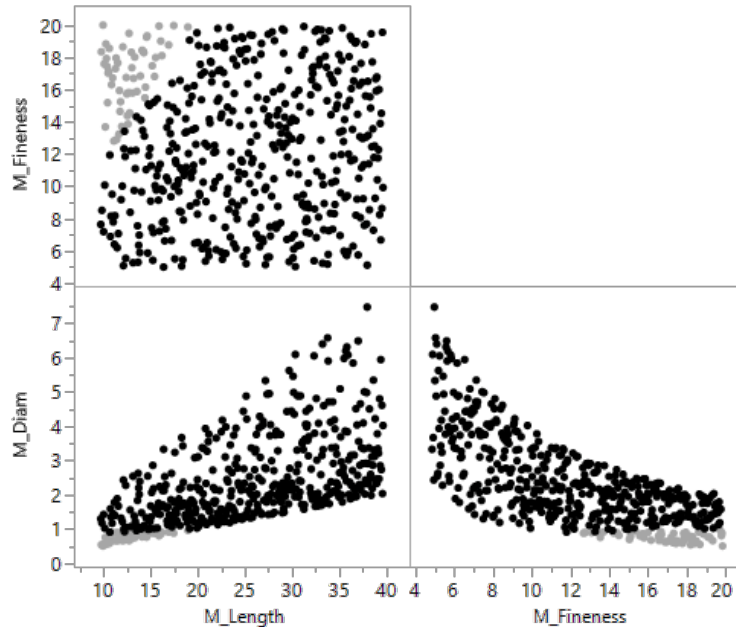


Fig. 12. Scatterplot matrix of missile length, missile fineness, and missile diameter highlighting payload diameter constraint

A constraint frontier occurs around a missile diameter of 1 ft. When a filter is applied to only include vehicles with a missile diameter equal to or greater than 1 ft, all 446 vehicles in the filter meet the payload diameter constraint, a 100% success rate as compared to 89.2% without excluding any viable vehicles. The same constraint frontier appears on the missile length versus missile fineness ratio scatterplot, though in the form of a diagonal line. This makes it difficult to downsize the missile length or missile fineness ratio DOE ranges without excluding viable vehicles.

The second result explored is whether the vehicles meet the fuel volume constraint. The fuel tank must have a positive volume, as discussed in Section VIII.B.2: Internal Geometry. If the design of the missile is such that the volume of the fuel tank is negative, then the vehicles does not meet the fuel volume constraint. Of the 500 vehicles ran, 331 met the fuel volume constraint, a 66.2% success rate. A constraint scatterplot showing the vehicles that meet or break the fuel volume constraint plotted against the missile length, missile fineness, nose fineness, and resulting

center body length is shown below in Fig. 13. Center body length is the total length of the missile minus the booster length and the nose length.

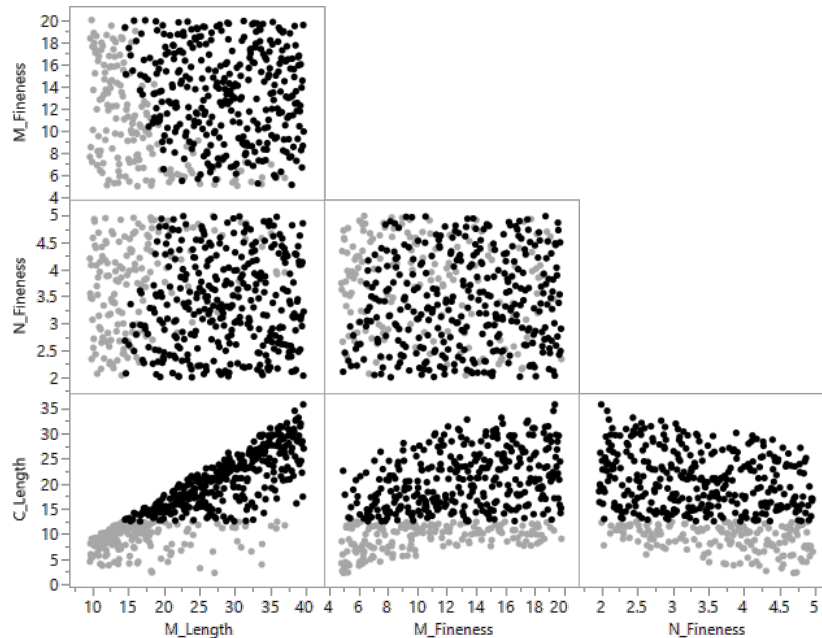


Fig. 13. Scatterplot matrix of missile length, missile fineness, nose fineness, and center body length highlighting fuel volume constraint

A constraint frontier occurs exactly at a center body length of 12.5 ft. This total is a consequence of the 3 ft required for the avionics package, the 3.5 ft required for the payload, and the 6 ft required for the ramjet. Another frontier appears on missile length around 15 ft, where there were no viable vehicles below 15 ft. When a filter is applied to only include vehicles with a missile length equal to or greater than 15 ft, 330 vehicles meet the fuel volume constraint out of 416 total vehicles in the filter, a 79.3% success rate as compared to the 66.2% while only excluding one successful vehicle. Missile fineness ratio and nose fineness ratio both contain diagonal frontiers, but no clear indication on how to limit their ranges to reduce the number of invalid vehicles without excluding viable vehicles.

The third result explored is whether the vehicles meet the stability constraint. The pitching moment coefficient derivative with angle of attack ($C_{m\alpha}$) must be negative for the missile to have longitudinal static stability. Therefore, if the vehicle design results in a $C_{m\alpha}$ that is positive, then the vehicle does not meet the stability constraint. Of the 441 vehicles that successfully ran through Missile Datcom without crashing, 134 met the stability constraint, a 30.4% success rate. A constraint scatterplot matrix showing the vehicles that meet or break the stability constraint plotted

against the missile length, missile fineness ratio, and resulting missile diameter and $C_{m\alpha}$ is shown below in Fig. 14. Another constraint scatterplot plotted against the total wing area, wing trailing edge percentage, total tail area, tail trailing edge percentage, and resulting $C_{m\alpha}$ is shown below in Fig. 15.

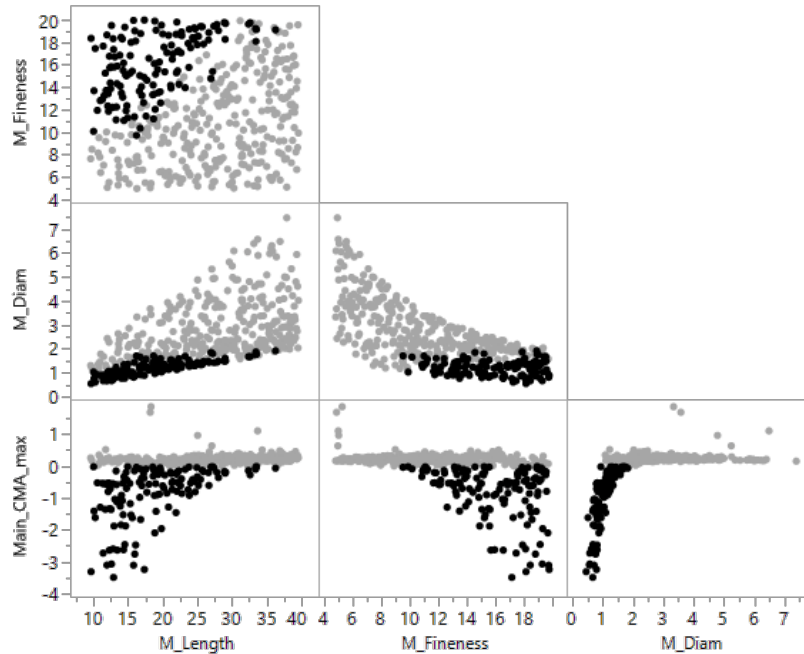


Fig. 14. Scatterplot matrix of missile length, missile fineness, missile diameter, and $C_{m\alpha}$ highlighting stability constraint

Three constraint frontiers are identifiable in Fig. 14: a missile length of 30 ft, a missile fineness ratio of 10, and a missile diameter of 2 inches. When a filter is applied to only include vehicles with a missile length equal to or less than 35 ft and missile fineness equal to or greater than 10, 132 vehicles meet the stability constraint out of 236 total vehicles in the filter, a 55.9% success rate as compared to 30.4% while only excluding 2 successful vehicles. Alternatively, when a filter is applied to only include the vehicles with a missile diameter equal to or less than 2 ft, 134 vehicles meet the stability constraint out of 247 total vehicles in the filter, a 54.3% success rate while excluding no successful vehicles. Surprisingly, no constraint frontiers appear for any of the fin sizing parameters in Fig. 15. This was unexpected as sizing and locations of the wing and tail were expected to be significant problems in properly stabilizing the missile. Instead, the geometry of the main body of the missile has the greatest effect on stability.

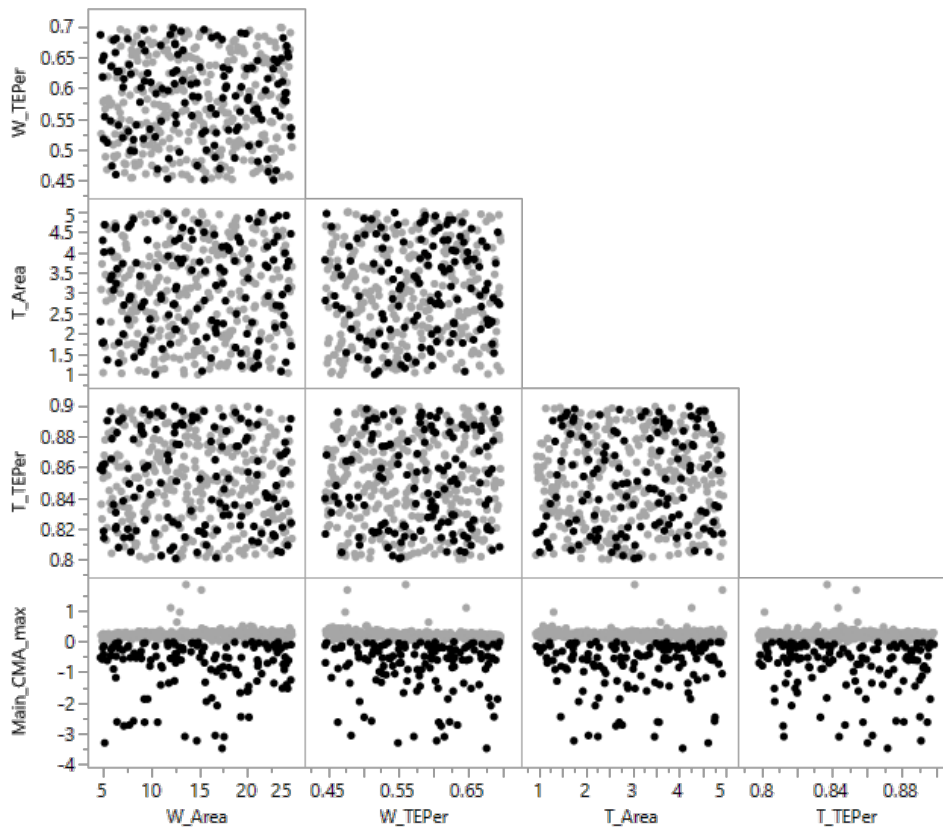


Fig. 15. Scatterplot matrix of wing area, wing trailing edge percentage, tail area, tail trailing edge percentage, and C_{ma} highlighting stability constraint

The fourth result explored is whether the vehicles meet the boost constraint. From testing the trajectory code, it was discovered that vehicles that are unable to achieve a speed of Mach 1.75 after the initial boost phase are unlikely to complete a successful cruise phase. Therefore, if the vehicle results in a booster termination speed of less than Mach 1.75, then the vehicle does not meet the boost constraint. Only vehicles that met both the diameter constraint and the fuel volume constraint were run through the boost phase. Of the 500 vehicles, only 321 met both constraints. Of the 321 vehicles, only 287 successfully ran through trajectory. Of the 287 vehicles that successfully ran through trajectory, 31 met the boost constraint, a 13.9% success rate. 256 of the vehicles were not able to meet the boost constraint while 34 vehicles resulted in the code failing, not providing any result. A constraint scatterplot matrix showing the vehicles that meet or break the boost constraint plotted against the missile length, missile fineness ratio, resulting missile diameter and resulting boost Mach number is shown below in Fig. 16. Another constraint scatterplot matrix plotted

against the solid booster stage length ratio, solid booster grain inner diameter ratio, resulting solid booster stage length, and resulting boost Mach number is shown below in Fig. 17.

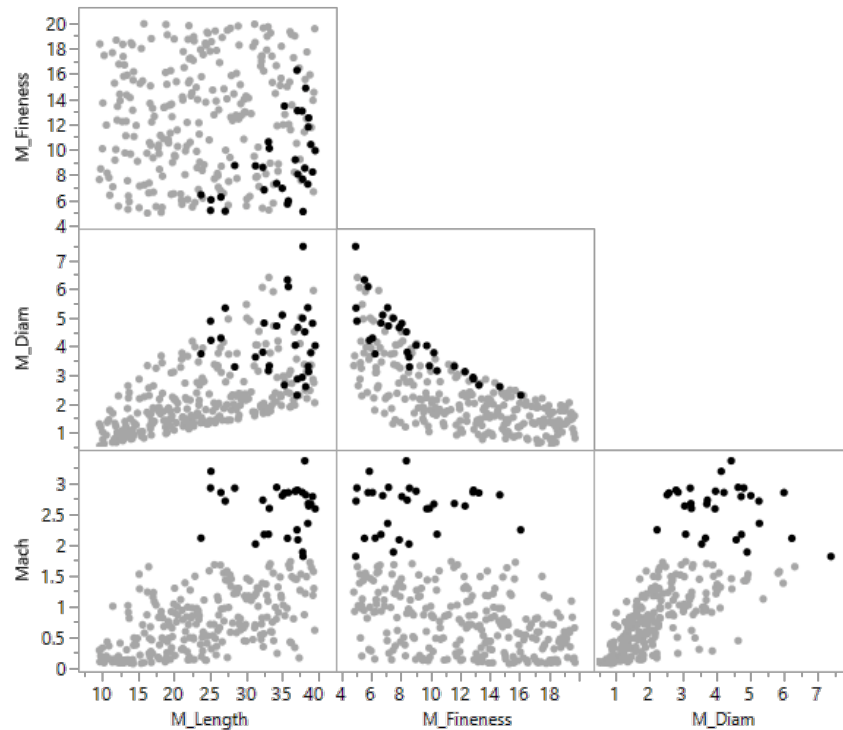


Fig. 16. Scatterplot matrix of missile length, missile fineness ratio, missile diameter, and boost Mach number highlighting boost constraint

Three constraint frontiers are identifiable in Fig. 16: a missile length of 25 ft, a missile fineness of 17, and a missile diameter of 2.3 ft. Two constraint frontiers are identifiable in Fig. 17: a solid stage length ratio of 0.15 and a stage length of 5 ft. When a filter is applied to only include vehicles with a missile length greater than or equal to 25 feet, a missile diameter greater than 2 ft, and a solid stage length ratio greater than or equal to 0.15, 31 vehicles meet the boost constraint out 90 total vehicles in the filter, a 34.4% success rate as compared to 13.9% without excluding a single successful vehicle.

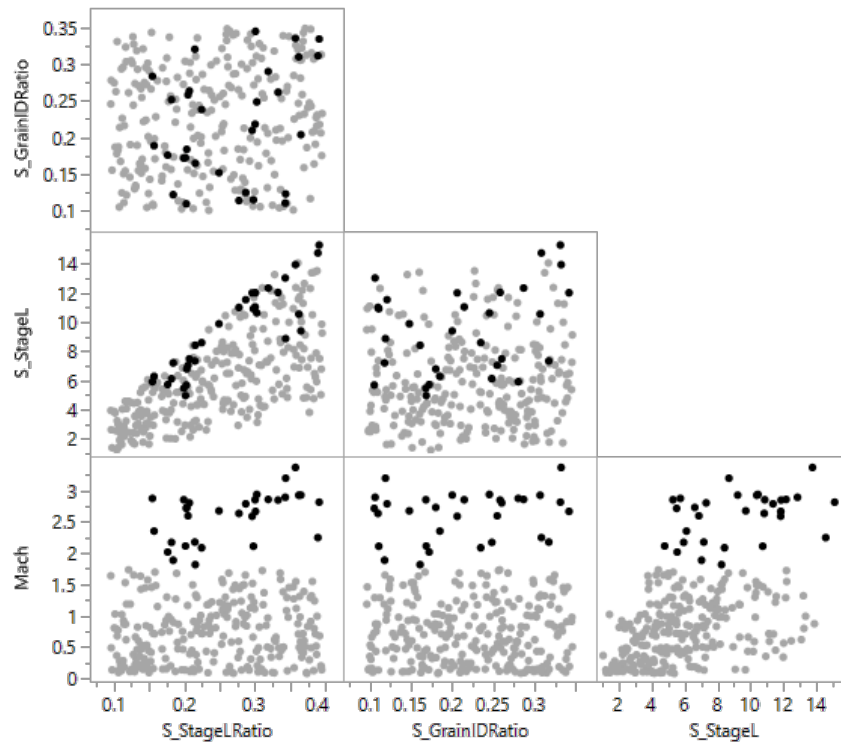


Fig. 17. Scatterplot matrix of solid booster stage length ratio, solid booster grain inner diameter ratio, solid booster stage length, and boost Mach number highlighting boost constraint

The final set of results explored were the overall performance of the missile. The primary metrics of interest were the range achieved by the high diver flight profile, the total missile weight, and then booster mass fraction. A scatterplot matrix showing the vehicles that were successfully able to complete the boost phase in black plotted against missile length, missile fineness ratio, resulting missile diameter, solid stage length ratio, and resulting solid stage length on the x-axis and range and total missile weight on the y-axis is shown below in Fig. 18.

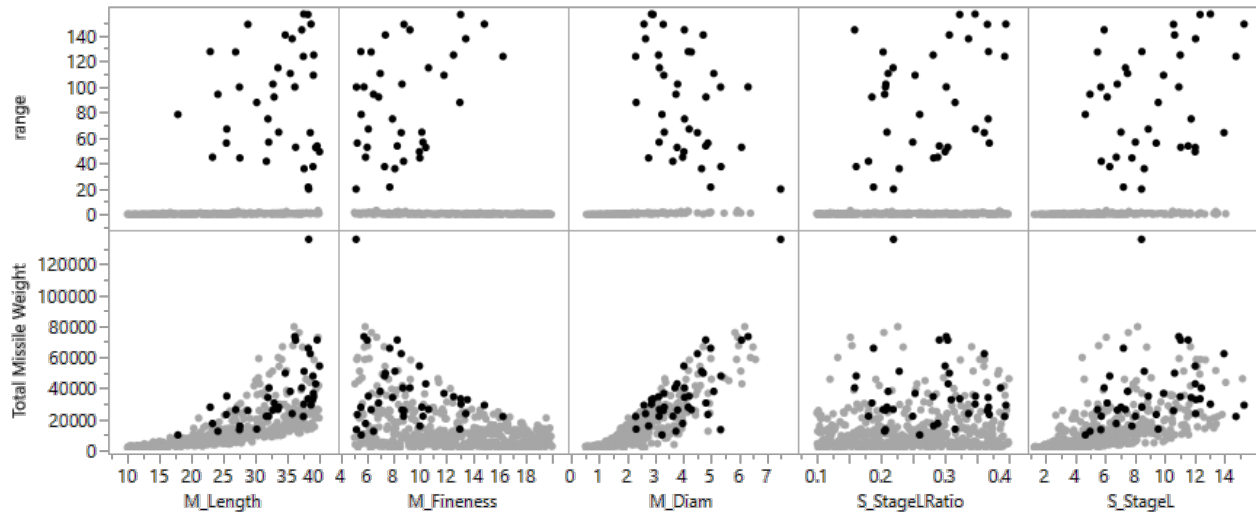


Fig. 18. Scatterplot matrix of missile performance metrics against significant DOE parameters

The range achievable by the missile designs are highly varied by the input parameters. The vehicles that were successfully able to achieve the necessary boost speed are distributed across the range spectrum without much clear distinction for their input parameters. The total missile weight, on the other hand, is highly tied to the input parameter. Both as missile length and missile diameter increase, the total missile weight increases. This is unsurprising as the missile getting larger is expected to make it heavier. As missile fineness ratio increases, the total missile weight decreases, mirroring the logical result from the missile length and missile diameter. Surprisingly, solid stage length ratio does not have a clear trend on the overall missile weight. Solid stage length does have a minor upwards trend, due to the fact it only effects the size of part of the missile.

Overall, the body sizing ranging experiment showed that a significant number of the vehicles were not viable. The number of vehicles that were able to meet each of the constraints is shown below in Table 8.

Table 8. Number of vehicles meeting constraints for body sizing ranging experiment

Constraint	Payload Diameter Constraint	Fuel Volume Constraint	Stability Constraint	Boost Constraint	All Constraints
Met	446	331	134	31	0
Failed	54	169	366	469	500

Out of all 500 vehicles, none were able to meet all the constraints. While there were no successful vehicles in the ranging experiment, the results can still be used to inform the ideal ranging of variables for future DOEs. Based on

the results from the constraint scatterplots, a new set of parameter ranges were established to reduce the number of unviable vehicles without significantly reducing the number of viable vehicles. In selected the new parameter ranges, missile fineness ratio was removed as a parameter and replaced with missile diameter. This is because including missile diameter as a parameter provides more accuracy in removing infeasible vehicle designs. Additionally, there are conflicting requirements by the stability and boost constraints. Stability requires that missile diameter be less than 2 ft while boost requires that missile diameter be greater than 2 ft. While stability is primarily affected by parameters that varied in the DOE, there were several parameters defaulted in the DOE that could affect the ability to meet the boost constraint, such as the solid booster stage diameter ratio. For that reason, missile diameter was set to a maximum of 2 ft to meet the stability requirements while a later design of experiments was run to explore how to meet the boost constraint, as discussed in Section VIII.C.2: Boost Phase The list of the changes to the parameter ranges is included below in Table 9.

Table 9. Parameter range updates from body sizing ranging experiment.

Parameter	Old Range		Updated Range	
	Minimum	Maximum	Minimum	Maximum
Missile Length	10 ft	40 ft	17 ft	30 ft
Missile Fineness Ratio	5	20	-	-
Missile Diameter	-	-	1.033 ft	2 ft
Solid Booster Stage Length Ratio	10%	40%	10%	80%

The vehicles from the body sizing ranging experiment that fit within the new parameter ranges were collected to see the results on the constraints. Of the 500 vehicles, 116 fall within the new ranges. The number of vehicles within the new parameter ranges meeting the constraints are shown below in Table 10.

Table 10. Number of vehicles meeting constraints for body sizing ranging experiment with updated ranges.

Constraint	Payload Diameter Constraint	Fuel Volume Constraint	Stability Constraint	Boost Constraint	All Constraints
Met	116	101	70	0	0
Failed	0	15	46	116	116

The restriction of the vehicles to only those within the updated parameter ranges significantly improves performance for the payload diameter constraint, fuel volume constraint, and stability constraint. Payload diameter

constrain compliance increases from 89.2% to 100%. Fuel volume constraint compliance increases from 66.2% to 87.1%. Stability constraint compliance has the greatest increase from 30.4% to 60.3%. Boost constraint has a decrease in compliance from 13.9% to 0%, which is to be expected given the limitations on missile diameter. Because of these improvements in constraint compliance, these ranges will be used in later DOEs.

B. Solid Booster Ranging Experiment

The objective of the solid booster ranging experiment was to obtain ideal sizing ranges for parameters of the solid booster. The parameters of interest are those related to the overall sizing and weight of the missile as well as the size and geometry of the solid booster. The ranges for the parameters are informed from the initial body sizing ranging experiment. The selected parameter and their ranges are shown below in Table 11. The parameters not selected for varying in the solid booster ranging experiment had to be set to a default value. The defaulted parameters are shown below in Table 11.

Table 11. Variables and ranges for body sizing ranging experiment.

Parameter	Minimum		Maximum	
Missile Length	15 ft		30 ft	
Missile Diameter	1 ft		2 ft	
Nose Fineness	2		5	
Solid Booster Stage Diameter Ratio	0.50		2.00	
Solid Booster Stage Length Ratio	0.10		0.50	
Solid Booster Geometry Type	Bates	Finocyl	Star	Starocyl
Solid Booster Grain Inner Diameter Ratio	0.05		0.50	
Solid Booster Fin Count	2		8	
Solid Booster Fin Width Ratio	0.01		0.10	

A DOE containing 500 sample vehicles was created in JMP. The vehicles were distributed using fast flexible filling, a space filling method capable of distributing continuous and categorical variables. The vehicles were run through the missile design environment up through the high diver boost phase, but not through the cruise phase.

The only constraint of concern for this ranging experiment is the boost constraint. Of the 500 vehicles ran, 343 successfully ran through trajectory without the code failing. Of the 343 vehicles that successfully ran through trajectory, 55 met the boost constraint, a 16.0% success rate. A constraint scatterplot matrix showing the vehicles that

meet or break the boost constraint plotted against missile length, missile diameter, solid stage diameter ratio, solid stage length ratio, and solid stage geometry type on the x-axis and boost Mach number on the y-axis is shown below in Fig. 19.

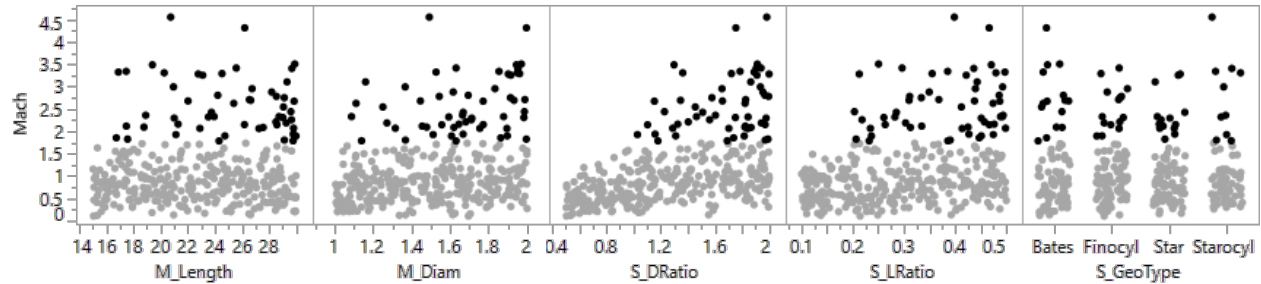


Fig. 19. Scatterplot matrix of missile performance metrics against significant DOE parameters.

Two constraint frontiers are identifiable in Fig. 19: a solid stage diameter ratio of 100% and a solid stage length ratio of 20%. When a filter is applied to only include the vehicles with a solid stage diameter ratio greater than or equal to 100% and a solid stage length ratio greater than or equal to 20%, 54 vehicles meet the boost constraint out of 166 vehicles in the filter, a 32.5% success rate as compared to 16.0% while only excluding one viable vehicle.

Based on the results from the constraint scatterplot, a new set of parameter ranges were established. Because of the possibility of viable results beyond the initial estimated parameter range, the new maximum solid booster stage length ratio was selected to be 0.80. The list of the changes to the parameter ranges is included below in Table 12.

Table 12. Parameter range updates from solid booster ranging experiment.

Parameter	Old Range		Updated Range	
	Minimum	Maximum	Minimum	Maximum
Solid Booster Stage Length Ratio	0.10	0.50	0.20	0.80
Solid Booster Stage Diameter Ratio	0.50	2.00	1.00	2.00

Because the minimum solid booster stage diameter ratio has been raised to 100%, any future vehicle will have a solid motor with a diameter as large as if not larger than the main missile. This means that the use of an integral rocket-ramjet is not a feasible configuration as the solid booster must be smaller than the diameter of the missile to fit within the ramjet. All potential designs in the final DOE must be external aft-drop off boosters.

C. Final Design of Experiments

The final DOE serves as the last DOE of the exploration process. The results of the final DOE will be used to select the final design. Based on the results of the ranging experiments, the parameters and ranges for the final DOE were selected. The parameters and ranges for the final DOE are shown below in Table 13.

Table 13. Variables and ranges for first design of experiments.

Parameter	Minimum			Maximum		
Missile Length	17 ft			30 ft		
Missile Diameter	1.033 ft			2 ft		
Nose Fineness Ratio	2			5		
Inlet-Wing-Tail Configuration	3/0/3	3/3/3	4/0/4	4/2/4	4/4/4	
Wing Total Area	5 ft ²			25 ft ²		
Tail Total Area	1 ft ²			5 ft ²		
Inlet Total Area	0.5 ft ²			3 ft ²		
Solid Booster Stage Length Ratio	0.20			0.80		
Solid Booster Stage Diameter Ratio	1.00			2.00		

A DOE containing 1,000 sample vehicles was created in JMP. The vehicles were distributed using fast flexible filling. All 1,000 vehicles were initially run through the pre-trajectory disciplines: geometry, propulsion, weights and structures, and aerodynamics. The number of vehicles that were able to make the various constraints during the pre-trajectory runs are shown below in Table 14.

Table 14. Number of vehicles meeting pre-trajectory constraints for final selection DOE.

Constraint	Payload Diameter Constraint	Fuel Volume Constraint	Stability Constraint	Pre-Trajectory Constraints
Met	1,000	855	821	765
Failed	0	115	179	235

All 1,000 vehicles were able to meet the payload diameter constraint. This is because DOE contained the missile diameter parameter instead of the missile fineness ratio parameter. The minimum missile diameter was set high enough that all vehicles were able to meet the constraint. 855 of the vehicles were able to meet the fuel volume constraint. This occurred primarily for vehicles with low missile lengths and high nose fineness ratios, however neither the missile

length nor nose fineness ratio ranges could be reduced without excluding valid configurations. Therefore, the ranges for the missile length and nose fineness ratios values was properly set for the fuel volume constraint. 821 of the vehicles were able to meet the stability constraint. This occurred primarily for vehicles with high missile diameters and high nose fineness ratios, however, as with the fuel volume constraint, neither parameter could be reduced without excluding valid configurations, meaning the parameter ranges were properly set. 765 of the vehicles met all the pre-trajectory constraints when applied together. These 765 vehicles were then run through the boost phase of the trajectory for both the sea skimming and high diver profiles. The number of vehicles able to make the boost constraints of between Mach 2 and Mach 4.5 are shown below in Table 15.

Table 15. Number of vehicles meeting boost constraints for final selection DOE.

Constraint	Sea Skimming Boost Constraint	High Diver Boost Constraint	Combined Boost Constraint
Exceeded	42	14	-
Met	189	230	171
Failed	534	521	594

Of the 765 vehicles to run through the boost phase, 189 were able to meet the boost constraint for the sea skimming flight profile and 230 were able to meet the boost constraint for the high diver flight profile. The sea skimming flight profile had 534 underperforming vehicles and 42 overperforming vehicles while the high diver flight profile had 521 underperforming vehicles and 14 overperforming vehicles. 171 vehicles were able to meet the boost constraints for both the flight profiles where 594 either underperformed or overperformed for at least one of the flight profiles. The 189 successful sea skimming vehicles and the 230 successful high diver vehicles were then run through the cruise and termination phases of the trajectories for their respective flight profiles. The number of vehicles able to make the range constraint of 60 nmi are shown below in Table 16.

Table 16. Number of vehicles meeting range constraints for final DOE.

Constraint	Sea Skimming Range Constraint	High Diver Range Constraint	Combined Range Constraint
Met	47	97	44
Failed	142	133	-

Of the 47 vehicles that made the sea skimming range constraint, 5 did not make the high diver boost constraint. All 5 of the vehicles were underperforming in the high diver boost phase, with Mach numbers below 2. Therefore, none of the 5 vehicles were initially run through the high diver cruise phase. Those 5 vehicles were manually passed through the high diver cruise phase, removing the Mach 2 boost constraint. Of the vehicles, 2 were successfully able to complete the high diver cruise phase and achieve the high diver range constraint while the other 3 vehicles were unsuccessful in completing the high diver cruise phase. Of the 97 vehicles that initially made the high diver range constraint, 45 did not make the sea skimming range constraint. All 45 of the vehicles were overperforming in the sea skimming boost phase, with Mach numbers above 4.5. This is the opposite problem encountered with the successful sea skimming vehicles. This is because the high diver boost phase is more demanding on the solid motors due to the need to gain altitude, requiring more energy be converted into potential energy. As the sea skimming boost does not gain significant altitude, the energy can be focused into kinetic energy, resulting in a higher speed. Mach 4.5 starts to encroach upon hypersonic flight, which the missile environment was not designed to handle due to the lack of aerothermal analysis. Additionally, the aerodynamic tables generated by Missile Datcom did not go beyond Mach 4.5. For that reason, none of the 45 vehicles were included in the final list of viable vehicles. In the end, 44 total vehicles were revealed as viable designs. A scatterplot matrix showing the viable alternatives in black plotted against a weight and range performance metrics is shown below in Fig. 20.

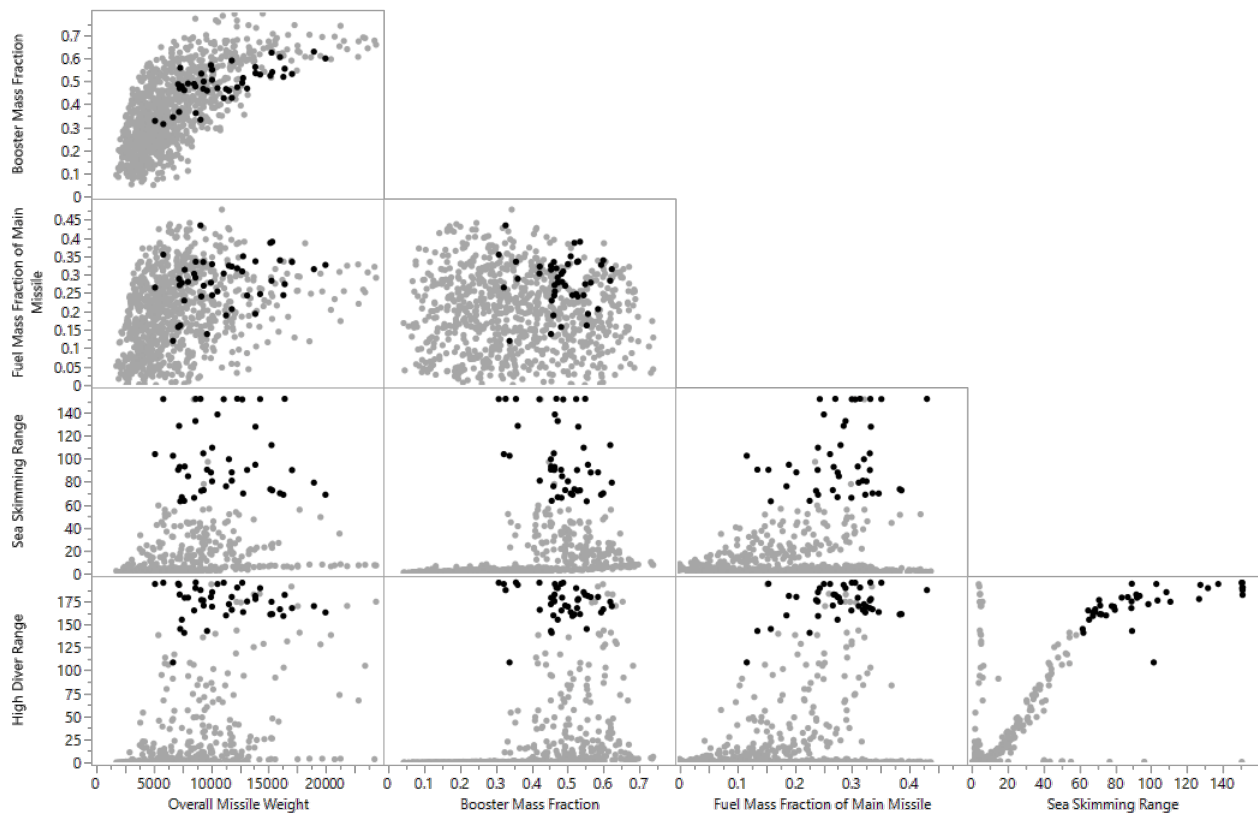


Fig. 20. Scatterplot matrix of missile performance metrics against significant DOE parameters.

Selecting a final design from the 44 viable vehicles requires a tradeoff between several competing performance characteristics. Of the 44 viable vehicles, no vehicle is the best for all the performance characteristics. Therefore, selecting a final design from the viable vehicles requires the use of a multi-attribute decision making (MADM) process. The MADM technique chosen was the Technique for Order Preference by Similarity to Ideal Solution (TOPSIS). TOPSIS works by identifying the best solution based on which alternative is the closest to a given positive ideal solution and the further from a given negative ideal solution. The positive ideal solution is a hypothetical solution with the most desirable criteria values out of the possible alternatives.

TOPSIS requires the identification of quantitative criteria to be used as objectives as well as whether they should be minimized or maximized as well as a relative weight. The sum of the weights of all the criteria must add up to 1. There are three primary performance characteristics to differentiate between the viable designs: overall missile weight, sea skimming range, and high diver range. Overall missile weight was selected as it is a surrogate for the total cost of the missile. Overall missile weight should be minimized. Overall missile weight was given a weighting of 0.5 because

of the important of making a cost-effective target missile. The sea skimming and high diver range were selected as the RFP describes an objective range of 150 nmi. Both ranges should be maximized. As both ranges are important to modeling different threats, the criteria were both given equal weights of 0.25. While metrics like booster mass fraction and liquid fuel mass fraction are important performance characteristics, they are not good metrics

The positive ideal solution (S^*) is found by taking the best possible value for each of the criteria. The negative ideal solution (S^-) is found by taking the worst possible value for of the criteria. The criteria values for the positive ideal solution and the negative ideal solution are shown below in Table 17.

Table 17. TOPSIS positive and negative ideal solutions.

Criteria	Overall Missile Weight	Sea Skimming Range	High Diver Range
Positive Ideal Solution	5,319 lbs.	152.3 nmi	195.8 nmi
Negative Ideal Solution	20,163 lbs.	63.1 nmi	108.8 nmi

To perform TOPSIS, the values of each attribute are normalized by the sum of squares of all the values for that criteria. Next, the relative importance is found by multiplying the normalized values by the criteria weights. Then, the Euclidean distances between the relative importance of each alternative and the relative importance of the positive and negative ideal solutions are found. Finally, the relative closeness (C^i) for each alternative is found by dividing the distance from the negative ideal solution by the sum of the distances to both the ideal solutions. The alternative with the highest C^i is the best alternative. A scatterplot matrix of the possible alternatives plotted on the three criteria is shown below in Fig. 21. The alternatives are colored based on their C^i value, with high C^i values shown in green and low C^i values shown in red. Additionally, the locations of the positive and negative ideal solutions are shown on each plot in the matrix.

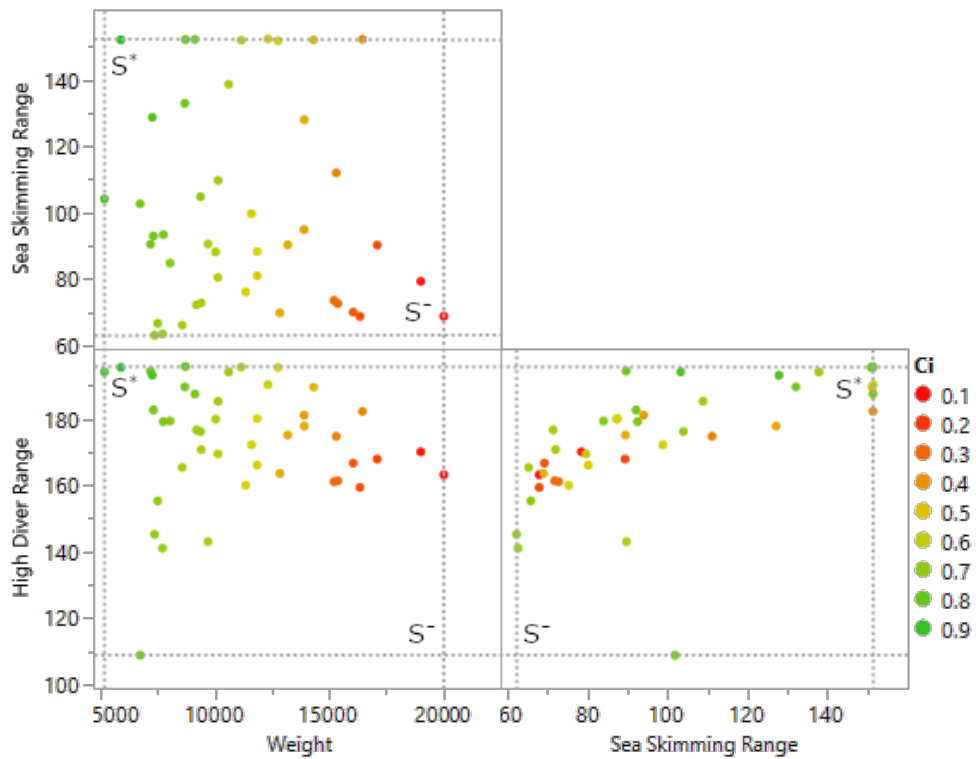


Fig. 21. Scatterplot matrix of missile performance metrics colored by TOPSIS performance.

The positive ideal solution appears in the top left of the weight vs high diver range and weight vs sea skimming range scatterplots due to the fact that weight is ideally minimized while it appears in the top right of the sea skimming range vs high diver range scatterplot. As designs approach the positive ideal solution in each of the scatterplots, their C^i approaches 1, though with some exceptions due to the multidimensionality of the problem. The top 5 performing TOPSIS alternatives as measured by C^i along with their criteria performance are shown below in Table 18.

Table 18. Top 5 TOPSIS alternatives.

Rank	Vehicle Number	C^i	Weight (lbs.)	Sea Skimming Range (nmi)	High Diver Range (nmi)
1	411	0.955	6,039	152.1	195.5
2	915	0.849	5,319	104.2	194.2
3	852	0.845	7,415	128.7	193.2
4	898	0.782	8,863	152.2	195.8
5	480	0.769	8,837	132.9	189.7

The standout best performing alternative is Vehicle 411. While it does not feature any highest performing attributes, it is only 0.2 nmi off from the maximum sea skimming range and 0.3 nmi off from the maximum high diver range. This is all accomplished while being the second lightest vehicle, only beaten out by the second place, Vehicle 915. Vehicle 915 is 720 lbs. lighter than Vehicle 411 and has a similar high diver range but underperforms in sea skimming range by 47.9 nmi. While Vehicle 915 may be an appealing alternative if weight was the absolute deciding factor, the competing desires of the three criteria makes Vehicle 411 the overwhelming top performer. For that reason, Vehicle 411 was selected as the final baseline.

D. Final Design Changes

From the final design of experiments, Vehicle 411 was selected as the architecture that performed the best against the design criteria for the high-diver and the surface skimming profile. However, it was found that in both the surface skimming and the high-diver flight profiles that the vehicle was able to achieve the objective range while having reserve fuel. Because it is a target missile that will land in a safe test range, there was no need to have fuel reserves. For this reason, final design changes were made such that no fuel would be left in reserve and be wasted upon terminal impact. The weight-capacity of the liquid fuel cell on Vehicle 411 was reduced by 250 lb_f to become the ASDL-1776 PROMISE. Table 19 shows the weight breakdown of the Vehicle 411, the best architecture from the design of experiments, and the ASDL-1776.

Table 19. Final Design Changes.

Weight (lbs.)	Vehicle 411	ASDL-1776
Launch Weight	6039.50	5789.50
Booster Weight	1901.80	1901.80
Main Body Weight	4137.70	3887.70
Ramjet Fuel Weight	1468.41	1218.41
Empty Weight	2669.28	2669.28

X. Results

Chapter IX identified the optimal missile architecture that is able achieve the objective ranges for the high-dive and the sea-skimming flight profiles, the ASDL-1776. The following sections will provide a detailed discussion on the properties and performance of the ASDL-1776.

A. Geometry

The geometry of the ASDL-1776 was taken from the DOE parameters used to define vehicle 411. Those parameters are shown below in Table 20. Additionally, the remaining geometric parameterization of the ASDL-1776 is shown below in Table 21.

Table 20. DOE parameters of the ASDL-1776.

DOE Parameter	Value
Missile Length	29.46 ft
Missile Diameter	1.496 ft
Nose Fineness Ratio	4.163
Inlet-Wing-Tail Configuration	4/0/4
Wing Total Area	2.562 ft ²
Tail Total Area	1.362 ft ²
Inlet Total Area	1.362
Solid Booster Stage Length Ratio	0.1322
Solid Booster Stage Diameter Ratio	1.464

Table 21. Remaining geometric parameters of the ASDL-1776.

Geometric Parameter	Value
Total Missile Length	33.35 ft
Nose Length	6.229 ft
Center Body Length	23.23 ft
Booster Length	3.894 ft
Booster Diameter	2.192 ft
Missile Fineness	19.69
Booster Fineness	1.776

A visual rendering of the final missile design, including all design features and the official ASDL-1776 PROMISE logo is shown below in Fig. 22.



Fig. 22. ASDL-1776 PROMISE visual rendering.

B. Weights and Structures

1. Weight and Center of Gravity

The selected missile design minimizes weight and has a stable CG location while meeting all trajectory requirements as stated in the RFP. Minimizing weight is a key design goal, as weight is a proxy for cost as shown in Section VI.G: Cost and Manufacturing Modeling, and CG location is critical to missile stability. The specifications for the selected missile are summarized in Table 22.

Table 22. Weight and CG results.

Mission Segment	Weight (lbs.)	Center of Gravity (ft from nose)
Launch	5,789.5	20.12
Solid Booster Burnout	4,204.6	16.10
Solid Booster Drop	3,887.7	14.93
Liquid Fuel Depletion	2,669.3	13.19

The weight results ensure that ASDL-1776 will meet all mission objectives and requirements without unnecessary weight, cost or complexity. The CG results ensure that the missile will remain in a stable configuration throughout the full mission. These results assume a full payload of 500 lbs. A variable payload was also simulated, showing the effect of payload weight on CG location during each mission segment. The results can be seen in the plots in Fig. 23, Fig. 24, Fig. 25, and Fig. 26 for launch, solid booster burnout, solid booster drop, and liquid fuel depletion, respectively.

The CG location moves further aft in each of the four cases as the payload departs from its maximum weight of 500 lbs. This is to be expected, as the payload is located towards the front end of the missile. However, since the payload is a relatively small proportion of the overall missile weight, the effect on CG is rather small. The largest difference between CG with full payload and CG with empty payload is the launch condition, where a CG shift of 0.864 ft (10.368 in) rearward is recorded as the payload is decreased from full weight to empty. This small CG shift should allow for a stable missile configuration even if a payload with less weight (or no payload at all) was flown.

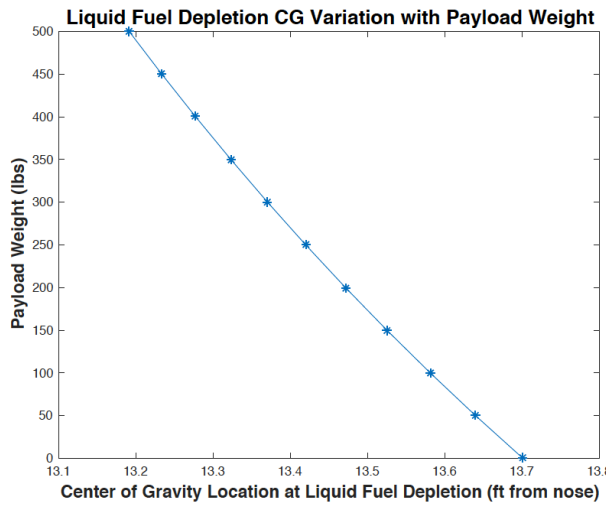


Fig. 23. Launch CG variation with payload weight.

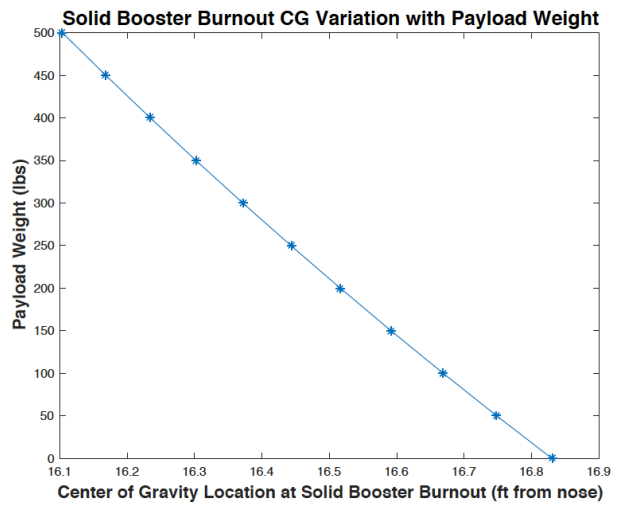


Fig. 24. Solid booster burnout CG variation with payload weight.

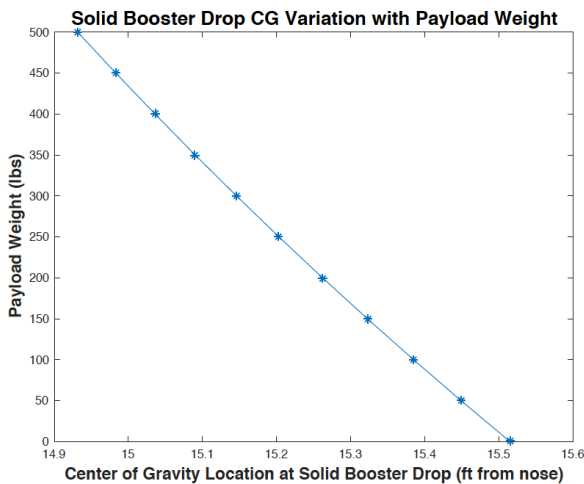


Fig. 25. Solid booster drop CG variation with payload weight.

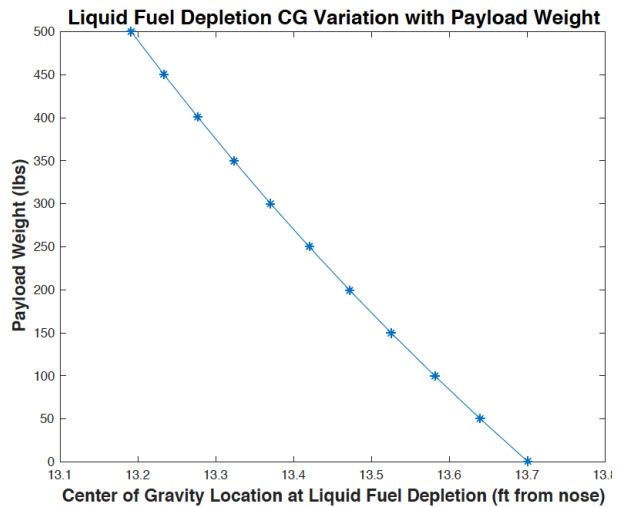


Fig. 26. Liquid fuel depletion CG variation with payload weight.

2. Stress Analysis

The results of the stress analysis gave necessary wall thickness of the overall missile body, the solid rocket booster casing, and the ramjet motor casing, as well as a factor of safety for each. The results are summarized in Table 23.

Table 23. Stress analysis results.

Component	Thickness (ft)	Factor of Safety
Missile Body	0.1818	1.5
Solid Booster Casing	0.1490	1.5
Ramjet Casing	0.2186	1.5

With the thicknesses shown above and a sufficient factor of safety for each of the casings, the missile can be considered capable of withstanding 15 g maneuvers without damage to the structure. Since 15 g is the maximum g-force that the missile is required to withstand per the RFP, ASDL-1776 will be capable of performing all necessary high g maneuvers [1].

C. Trajectory

The trajectory was analyzed using two different codes, tailored specifically to be able to handle their respective flight profiles. With BrahMos being the most formidable adversary in operations, and the GQM-163a Coyote being a current target missile; the flight trajectories were defined to have similar or improved operations. As referenced in Section V.I.B: Motivation and Existing Systems, BrahMos is capable of Mach 3 at 50,000 ft for a high dive profile, and down below 250 ft at what is likely a slower speed. The Coyote is capable of Mach 3-4 at 55,000 ft or around Mach 2.6 in a sea-skimming flight profile.

1. High Dive Flight Profile

For the high-dive profile, the target cruise speed was set to Mach 3.25 with a cruise altitude of 50,000 ft. This places the designed capabilities within the realm of the Coyote and being faster the openly reported speed of the BrahMos missile. To characterize the flight profile of the ASDL-1776 missile, Fig. 27 through Fig. 30 show the altitude, range and velocity time history during the flight. The boost phase achieves Mach 2.05, which provides a safe ramjet ignition condition to avoid a failed-ignition or flameout during the early stages of the cruise phase. Once in the cruise phase, the missile climbs to achieve the trajectory design altitude of 50,000 ft and reach the cruise speed of Mach 3.25. During the dive phase of the trajectory, the missile has a terminal impact speed of Mach 2.99 with terminal dive angle of 74.5 degrees. The total flight time for the high dive trajectory is 386.5 seconds for an untrained range of 182.16 nmi. Meaning the trajectory can be refined such that the missile will hit the 150 nmi range target. The time to cruise altitude is 37.5 seconds.

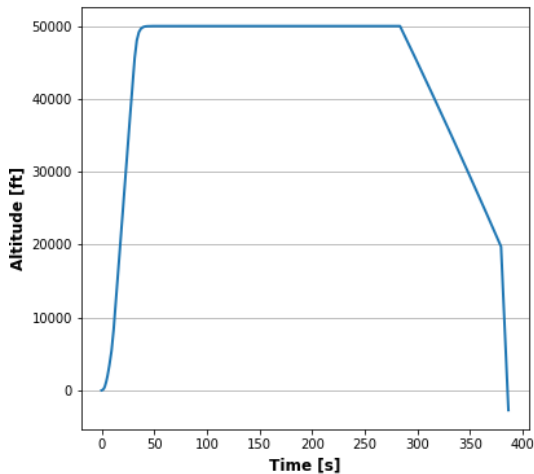


Fig. 27. Time history of high dive flight altitude.

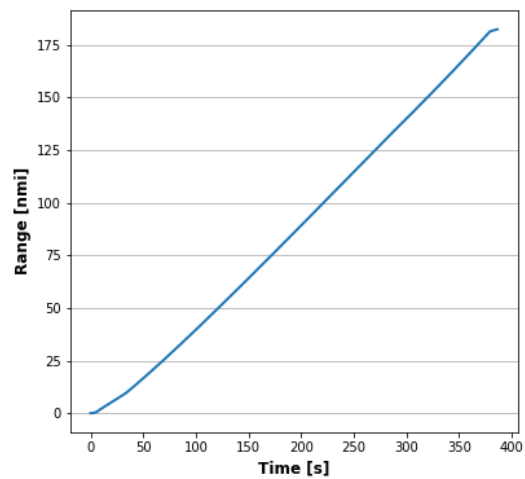


Fig. 28. Time history of high dive range.

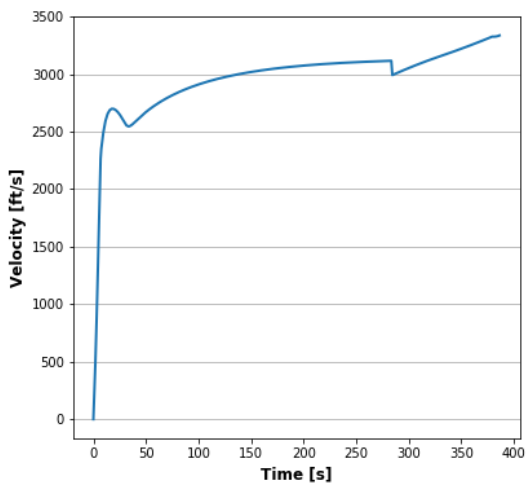


Fig. 29. Time history of high dive velocity.

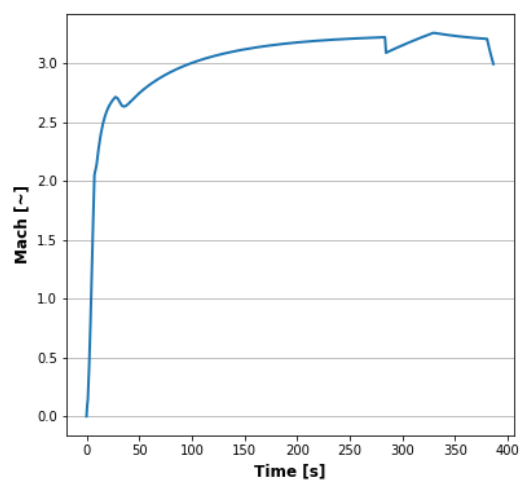


Fig. 30. Time history of high dive Mach number.

During the propagation of the trajectory, mass flow and the launch weight mass fraction are used to determine when the rocket motor and the ramjet burnout occurs. Fig. 31 and Fig. 32 show the flight time histories of the overall weight, and the propellant mass flow. At the flight time 7.5 s, the rocket motor burnouts out and the booster is dropped. The empty weight of the missile is 2669.28 lb_f while the high diver profile ends at impact weight of 3274 lb_f. At full fuel capacity the missile has an excess fuel capacity of 604.7 lb_f so the launch crew can choose to not fill the liquid fuel to full capacity for the operation of a high-dive missile defense training flight.

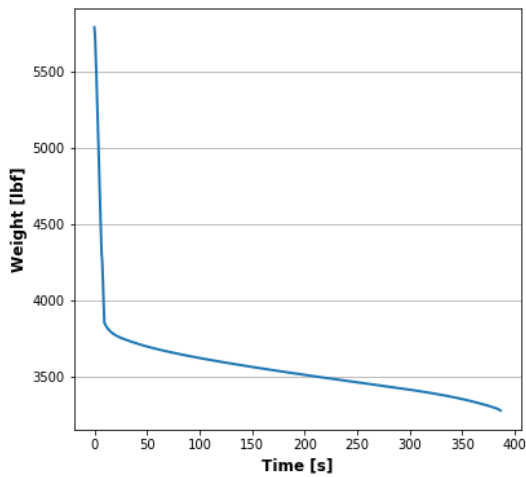


Fig. 31. Time history of high dive overall weight.

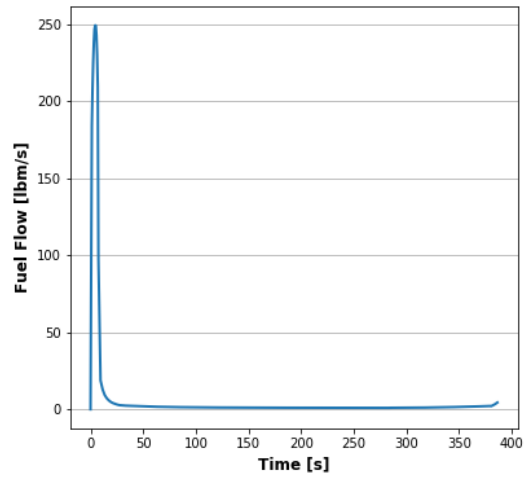


Fig. 32. Time history of high dive fuel mass flow.

Fig. 33 shows the Thrust to weight and lift to drag ratios during the boost phase, and Fig. 34 shows altitude versus range. To size the launch rail length, the missile length of 29.5 ft will be used for reference. From ignition, the missile takes 0.3 seconds to travel 29.5 ft. At this point the thrust to weight ratio is 1.5 so the booster can support the missile during flight without requiring the stability of the rail. This argument is supported by Fig. 35, showing that missile continues to travel along a nearly constant flight path. For a high dive profile, the launch rail can be set to 29.5 ft with a launch azimuth of 45° . Fig. 35 shows the time history of the flight angle of attack, pitch angle and flight path angle. Fig. 36 shows aerodynamic and propulsive forces. Using the Bates grain geometry, the maximum thrust of the rocket motor was about 63,200 lb_f with a thrust to weight ratio of 13.4 occurring about 2 seconds before burnout. During the cruise phase the flight path angle and the angle of attack was solved to maintain a constant altitude. The thrust was defined to accelerate from the boost phase to Mach 3.25 and then sustain a velocity of Mach 3.25.

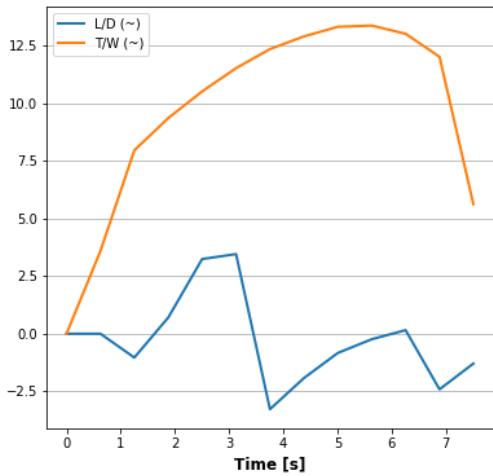


Fig. 33. High dive thrust to weight and lift to drag ratios during boost phase.

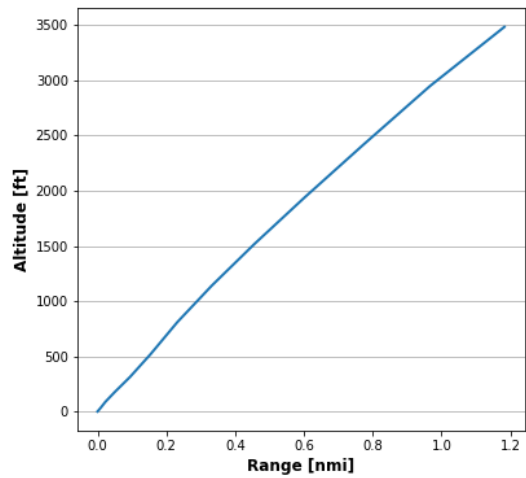


Fig. 34. High dive altitude vs range.

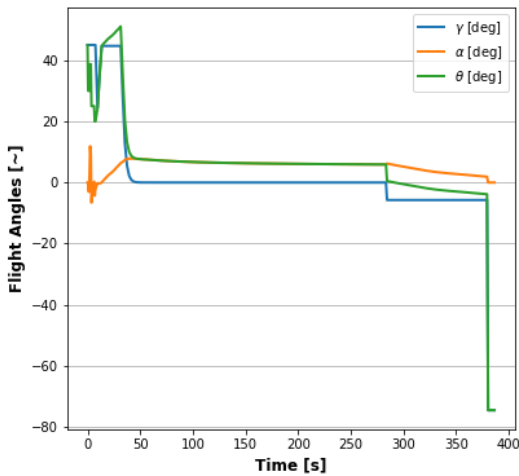


Fig. 35. High dive time history of flight angle of attack, pitch angle, and flight path angle.

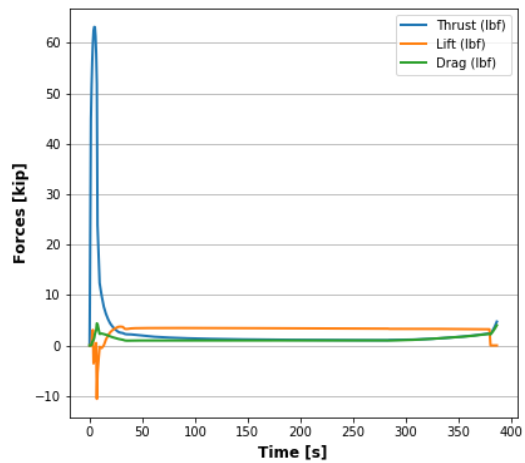


Fig. 36. High dive aerodynamic and propulsive forces.

Fig. 37 and Fig. 38 shows the flight trajectory and Mach number for a high dive with a terminal phase occurring immediately after reaching the cruise altitude. The missile has a time to cruise altitude of 37.5 seconds, and under the 75° dive angle constraint has an early-impact range of 13.5 nmi.

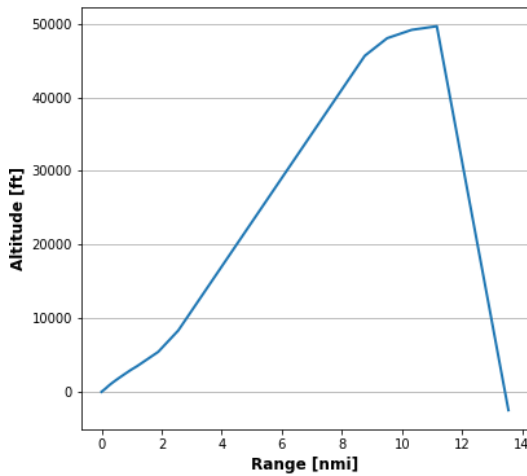


Fig. 37. Flight trajectory for high dive.

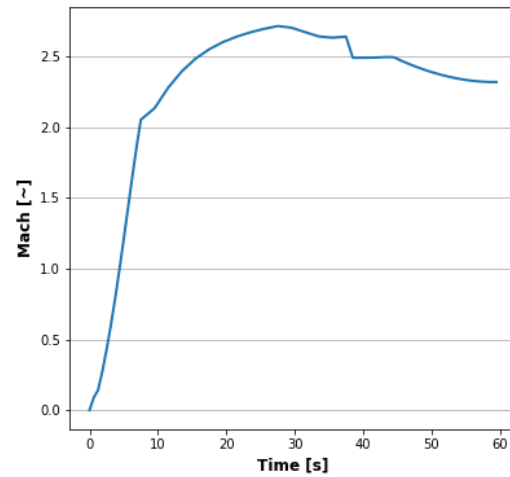


Fig. 38. Mach number for high dive.

2. Sea Skimming Flight Profile

For the high-dive profile, the target cruise speed was set to Mach 2.75 with a cruise altitude of 195 ft. This places the designed capabilities within the realm of the Coyote and being faster the openly reported speed of the BrahMos missile. To characterize the flight profile of the ASDL-1776 missile, Fig. 39 through Fig. 42 show the altitude, range and velocity time history during the flight. The boost phase achieves Mach 2.23, which provides a safe ramjet ignition condition to avoid a failed-ignition or flameout during the early stages of the cruise phase. For a Mach 2.75 at 195 ft cruise phase, the missile is capable achieving a range of 151.8 nmi range with a 313.9 second flight time. The terminal impact speed of the missile is Mach 2.6.

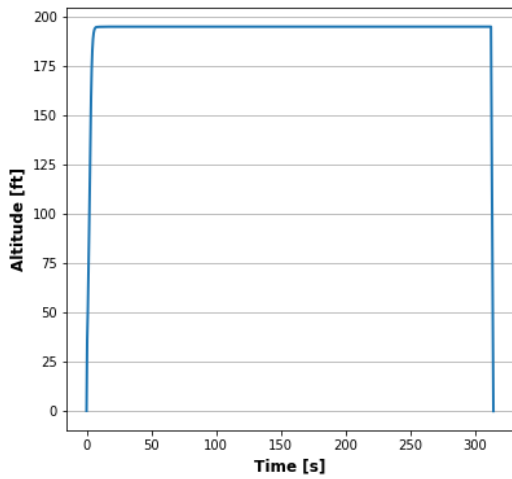


Fig. 39. Time history of sea skimming flight altitude.

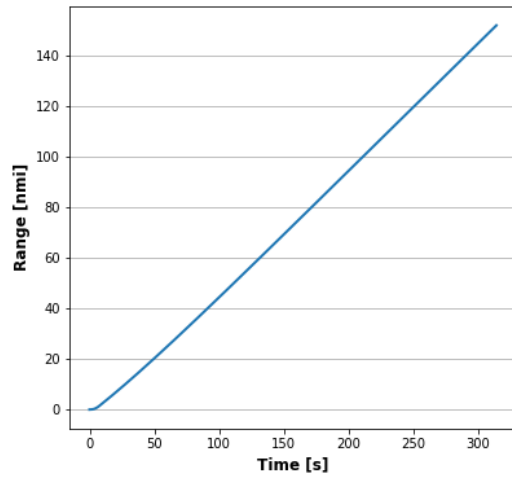


Fig. 40. Time history of sea skimming range.

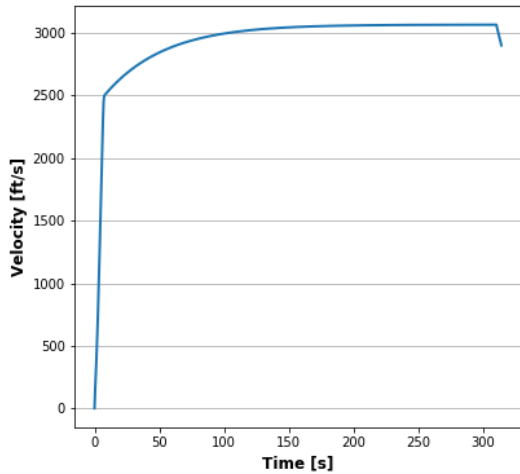


Fig. 41. Time history of sea skimming velocity.

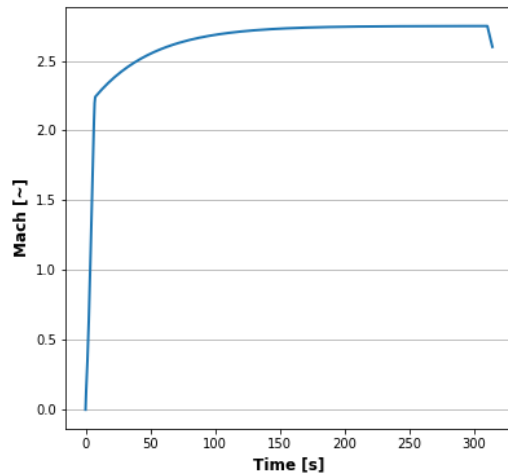


Fig. 42. Time history of sea skimming Mach number.

The sea skimming profile also used the mass flow and the launch weight mass fraction to determine when the rocket motor and the ramjet burnout occurred. Fig. 43 and Fig. 44 show the flight time histories of the overall weight, and the propellant mass flow. At the flight time 7.5 sec, the rocket motor burnouts out and the booster is dropped. The empty weight of the missile is 2669.28 lb_F while the sea skimming profile ends at impact weight of 2683 lb_F so the sea skimming profile is at the maximum range possible. During the sea skimming profile, the ambient density of the air is higher, resulting in a higher drag and trust requirement. For this reason, the sea skimming profile became the trajectory profile that had a larger impact on the sizing of the ramjet fuel tank.

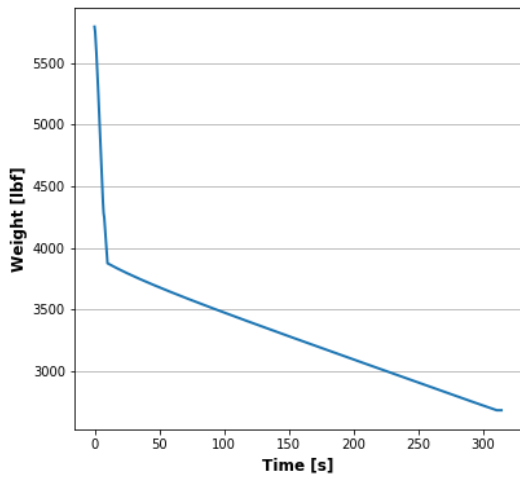


Fig. 43. Time history of sea skimming overall weight.

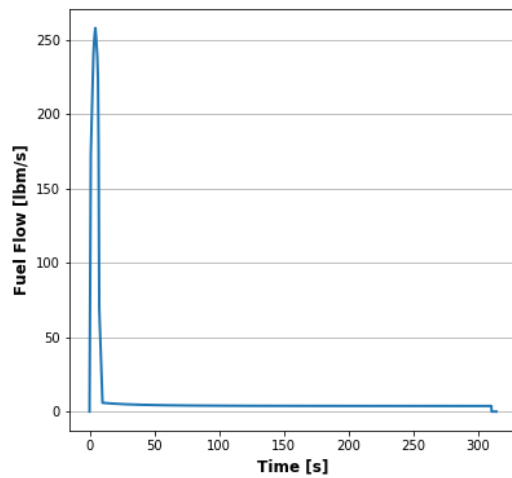


Fig. 44. Time history of sea skimming fuel mass flow.

Fig. 45 shows the Thrust to weight and lift to drag ratios during the boost phase, and Fig. 46 shows the altitude versus range plot. The rail length requirement for the sea skimming profile follows the same method as the high-dive rail length. This argument is supported by Fig. 47, showing that missile continues to travel along a nearly constant flight path angle. For a sea skimming profile, the launch rail can be set to 29.5 ft with a launch azimuth of 12.5 degrees. Fig. 47 shows the time history of the flight angle of attack, pitch angle and flight path angle. Fig. 48 shows aerodynamic and propulsive forces.

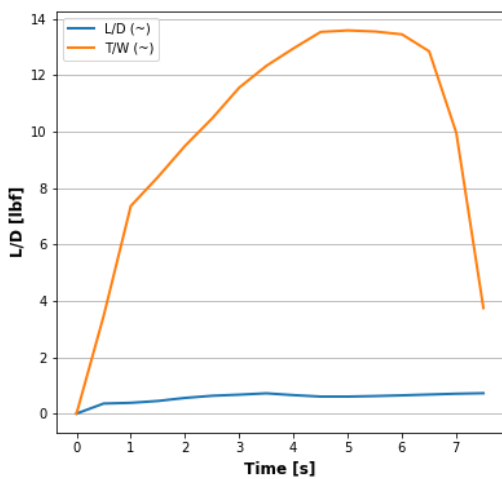


Fig. 45. Sea skimming thrust to weight and lift to drag ratios during boost phase.

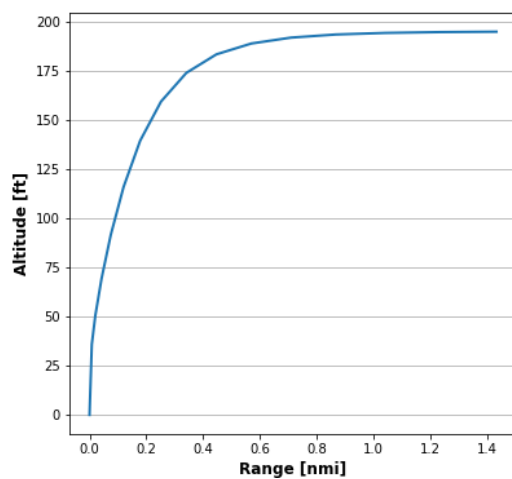


Fig. 46. Sea skimming altitude vs range.

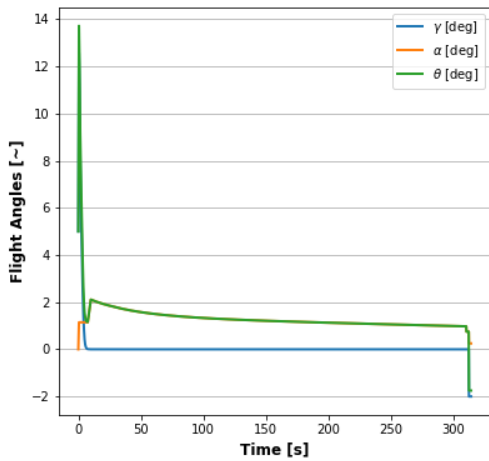


Fig. 47. Sea skimming time history of flight angle of attack, pitch angle, and flight path angle.

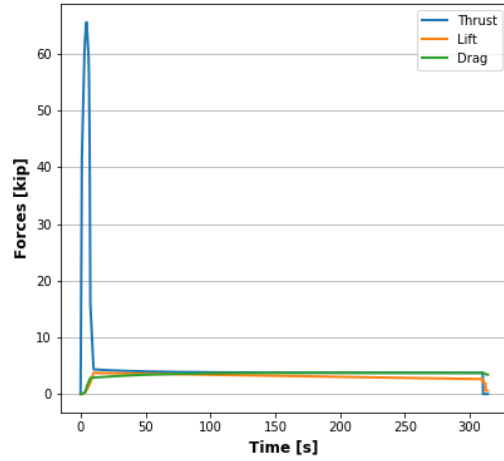


Fig. 48. Sea skimming aerodynamic and propulsive forces.

3. Varied Operating Conditions

To be capable of operating at multiple test sites, ASDL-1776 was also tested against different launch altitudes. Fig. 49 shows the high diver trajectory for the sea level launch altitude, and Fig. 50 shows the trajectory for the 3,500 ft launch altitude. With a lower ambient density, the booster is able to achieve Mach 2.08 at burnout; a small increase from the Mach 2.05 burnout during the launch at sea level.

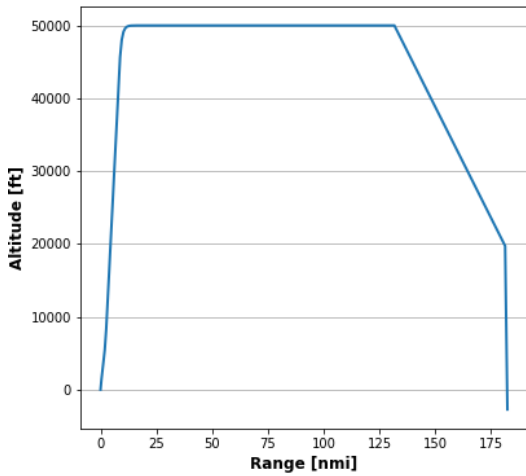


Fig. 49. High diver flight trajectory for sea level launch altitude.

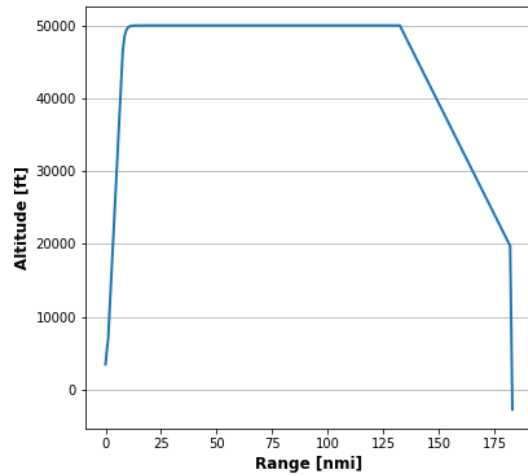


Fig. 50. High diver flight trajectory for 3500 ft launch altitude.

4. Trajectory Summary

The goal of the trajectory analysis was to verify that the missile is capable of the flight profile requirements laid out by the RFP. For a target missile to be effective for training defense systems, the missile should be capable of flight profiles similar or better than available data for existing weapon systems. Table 24 shows how ASDL-1776 performs against the trajectory requirements.

Table 24. Performance compared to Brahmos and trajectory requirements.

Requirement	Requirement	BrahMos	ASDL-1776 PROMISE
High Dive Range	60 nmi - 150 nmi	150 nmi	182+ nmi
High Dive Cruise Speed	Mach 2 – 4.5	Mach 3	Mach 3.25
Terminal Dive Angle	10°-75°	Steep-dive	74.5°
High Dive Terminal Impact Speed	Mach 0.9 - 3.5	~	Mach 2.99
Sea Skimming Range	60 nmi - 150 nmi	150 nmi	151.8 nmi
Sea Skimming Cruise Speed	Mach 2 – 3.5	n/a	Mach 2.75
Sea Skimming Impact Speed	Mach 2 - 3.5	~	Mach 2.6
Rail Length	~	~	29.5 ft
Launch Azimuth	0° - 90°	~	High Dive: 45° Sea Skimming: 12.5°
Launch Altitude	0-3500 ft		Capable of 0-3500 ft

D. Cost and Operations

The total cost of the ASDL-1776 PROMISE target missile system is based on the per unit costs and the launch system with all associated maintenance costs. At the weight of 5789 lbs. the first unit will have an estimate cost of \$2,211,500 while the last unit in the production run will cost \$902,020 due to the assumed learning curve, shown in Fig. 51. This gives an average cost per unit of \$1,060,900 and a total cost of \$387,230,000 2020 USD for the entire production run of 365 units.

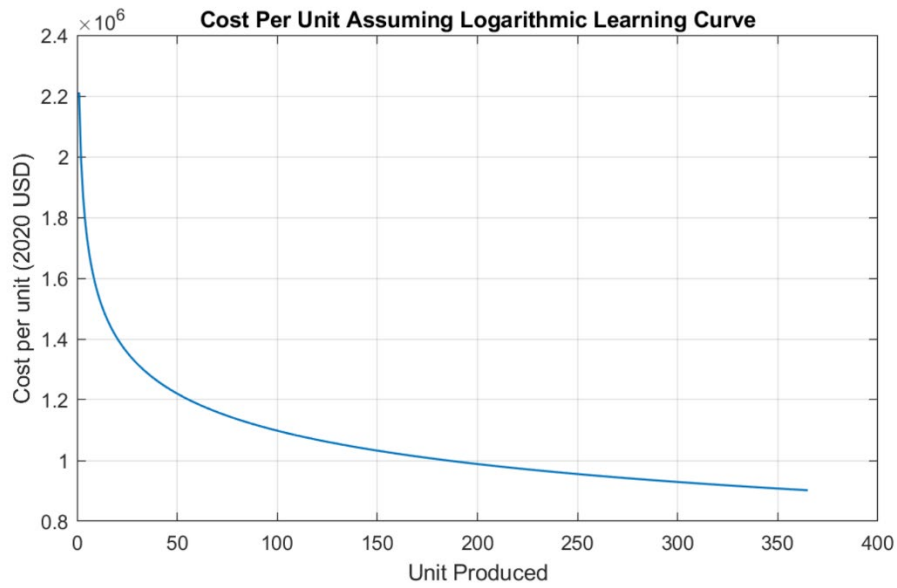


Fig. 51. Production cost per unit.

Operational costs were estimated using those of Standard Missile SM-6 due to its similar size, ability and low maintenance requirements [23]. Costs were scaled to the average per unit cost of each missile. The estimate assumed every missile in the production run was stored for the maximum 10 years to be an estimate of the maximum possible program cost. The 15 units used for developmental testing were not factored into the operational costs. All operational costs are enumerated in Table 25 below.

Table 25. Operational costs.

Cost Element	Average Annual Cost	Multiplier	Total Cost	Percent
Unit Operations	\$3000 per unit	350 Missiles * 10 years	\$10,500,000	35.2%
Maintenance	\$3200 per unit	350 Missiles * 10 years	\$11,200,000	37.6%
Sustaining Support	\$2100 per unit	350 Missiles * 10 years	\$7,350,000	24.7%
Indirect Support	\$200 per unit	350 Missiles * 10 years	\$700,000	2.4%
Total Operational Costs	~	~	\$29,750,000	100%

The total life cycle cost of the ASDL-1776 PROMISE is therefore estimated to be \$416,950,000 including the production run and all associated operational costs making it significantly less expensive than missiles of similar capabilities. This is shown below in Table 26.

Table 26. Total life cycle costs.

Component	Unit Cost (2020 USD)	Total Cost (2020 USD)	Percent
PROMISE	\$1,060,900	\$387,200,000	92.7%
Operational Costs	\$85,000	\$29,750,000	6.3%
Total Cost	\$1,145,900	\$416,950,000	100%

XI. Conclusion

The ASDL-1776 PROMISE missile provides a platform capable of high dive flight profiles with cruise speeds up to Mach 3.25 at 50,000 ft above sea level with a maximum range exceeding 180 nmi. It is also capable of sea skimming profiles with cruise speeds of Mach 2.75 at 195 ft above sea level with a maximum range of 150 nmi. This mission versatility makes the ASDL-1776 an ideal vehicle to be used for the development or training of defense systems against the expanding market of high kinetic energy aerial targets. Compared with the publicly available data, ASDL-1776 was designed to exceed the Mach 3 cruise speed that BrahMos is capable of in the high-diver profile. A target missile should be less expensive than the systems that air defenses are being trained against. BrahMos, the current leading cruise missile, has a reported unit cost of \$2.73M [24]. The acquisition price of the ASDL-1776 is only \$1.06M, which is less than 40% of the cost of a BrahMos missile. While being designed for same flight profiles as BrahMos, the ASDL-1776 PROMISE missile provides a target platform that is faster while being available at a significantly reduced cost compared to an operational weapon system.

A. Specification Compliance

Table 27 give the color chart that corresponds to Table 28, which shows the requirements laid out by the Request for Proposal alongside the capabilities that the ASDL-1776 PROMISE provides. This will provide the sections where the analysis is performed, along with showing whether or not the design satisfies each of the requirements.

Table 27. Compliance color chart

Color	Compliance
	Met objective requirement
	Met threshold requirement
	Did not meet requirements

Table 28. Specification Compliance

Specific Requirements from RFP	ASDL-1776 PROMISE Performance	Objective Met (Objective/Threshold/No)	Analysis Location
The target system shall be capable of achieving a threshold range of 60 nautical miles and an objective range of 150 nmi at the end of the terminal phase.	<i>High Diver:</i> 182+ nmi <i>Sea Skimming:</i> 152 nmi	Yes	<i>High Diver:</i> Section X.C.1 <i>Sea Skimming:</i> Section X.C.2
The target system shall be capable of operating between sea level and a maximum altitude of 65,000 feet.	ASDL-1776 is capable of High Dive and Sea Skimming profiles	Yes	<i>High Diver:</i> Section X.C.1 <i>Sea Skimming:</i> Section X.C.2
The target system shall be capable of performing high altitude “high diver” and low altitude “nap of the earth” or “sea skimming” flight profiles employed by threat supersonic cruise missiles.	ASDL-1776 is capable of High Dive and Sea Skimming profiles	Yes	<i>High Diver:</i> Section X.C.1 <i>Sea Skimming:</i> Section X.C.2
The target system shall be capable of cruising between 5,000 and 65,000 feet while in "high diver" flight profile.	50000 ft	Yes	Section X.C.1
The target system shall be capable of cruising between Mach 2.0 and Mach 4.5 while in "high diver" flight profile.	Mach 3.25	Yes	Section X.C.1
The target system shall be capable of performing a terminal diver between 10° and 75° while in "high diver" flight profile.	-74.5°	Yes	Section X.C.1

Specific Requirements from RFP	ASDL-1776 PROMISE Performance	Objective Met (Objective/Threshold/No)	Analysis Location
The target system shall be capable of an impact speed between Mach 0.9 and Mach 3.5 while in "high diver" flight profile.	Mach 2.99	Yes	Section X.C.1
The target system shall be capable of cruising between 15 and 200 ft above the surface while in "sea skimmer" flight profile.	195 ft	Yes	Section X.C.2
The target system shall be capable of cruising between Mach 2.0 and Mach 3.5 while in "sea skimmer" flight profile.	Mach 2.6	Yes	Section X.C.2
The target system shall be capable of performing terminal high-g maneuvers during the final 20 nmi of the trajectory while in "sea skimmer" flight profile.	15 g Lateral Turns 7g Vertical Turns Maneuver Duration 45s	Yes	Section X.B.2
The target system shall be capable of an impact speed between Mach 2.0 and Mach 3.6 while in "sea skimmer" flight profile.	Mach 2.6	Yes	Section X.C.2
The target system shall be capable of maintaining course within ± 1500 feet of the programmed trajectory.	± 1500 ft	Yes	Section VIII.F.6
The target system shall be capable of achieving a 50-foot Circular Error Probable (CEP) at the end of the terminal phase.	50 ft	Yes	Section VIII.F.6
The target system shall be capable of safe storage, transportation, and handling for at least 10 years without maintenance.	ASDL-1776 is capable of being stored for 10+ years without maintenance	Yes	Section VIII.H

Specific Requirements from RFP	ASDL-1776 PROMISE Performance	Objective Met (Objective/Threshold/No)	Analysis Location
The target system shall be capable of launching from a launch rail at a fixed ground site between 0- and 3,500-foot altitude.	Altitude: 0 ft – 3500 ft Elevation: 45° HD Elevation: 12.5° SS	Yes	Section X.C.3
The target system shall be compatible with modular payloads.	ASDL-1776 is capable of flying with a modular payload	Yes	Section X.B.1

XII. Acknowledgments

Thank you to our academic advisor, Dr. Dimitri Mavris, our faculty advisor, Dr. Bradford Robertson, our air breathing propulsion advisor, Dr. Andrew Yatsko, and the AIAA committee for providing guidance and feedback throughout the course of the project. Thank you to all the judges who took the time to read this report.

XIII. References

- [1] “2019-2020 Graduate Team Missile Systems Design Competition - Supersonic Aerial Target”, *American Institute of Aeronautics and Astronautics*. [online RFP] Available: <https://www.aiaa.org/get-involved/students-educators/Design-Competitions>
- [2] “BRAHMOS Supersonic Cruise Missile – BrahMos.com”, *Brahmos.com*. Available: <http://www.brahmos.com/content.php?id=10&sid=10>
- [3] “Chinese Mining Firm turns Cruise Missile Developer – Asian Military Review”, *Asian Military Review*. Available: <https://asianmilitaryreview.com/2019/01/chinese-mining-firm-turns-cruise-missile-developer/>
- [4] “Press Releases :: BRAHMOS missiles successfully test-fired from land and air platforms”, *Brahmos.com*. Available: <http://www.brahmos.com/pressRelease.php?id=90>
- [5] Barnes, T., “U.S. Navy Aerial Target Systems,” NDIA Symposium, Orlando, FL, October 2012. Available: <https://ndiastorage.blob.core.usgovcloudapi.net/ndia/2012/targets/TBarnes.pdf>
- [6] Parsch, A., “Raytheon (Beech) KD2B/Q-12/AQM-37, Raytheon AQM-37,” Designation Systems. Available: www.designation-systems.net/dusrm/m-37.html

- [7] “GQM-173A Multi-Stage Supersonic Target (MSST),” Global Security. Available: <https://www.globalsecurity.org/military/systems/munitions/gqm-173.htm>
- [8] Giangreco, L., “US Navy Searching for New Supersonic Aerial Target,” Flight Global. Available: www.flightglobal.com/news/articles/us-navy-searching-for-new-supersonic-aerial-target-439973/
- [9] “Brahmos Missiles,” The Hans India. Available: <https://www.thehansindia.com/posts/index/Education-and-Careers/2015-08-12/Brahmos-Missiles/169367>
- [10] Keller, J., “Northrop Grumman to build 15 GQM-163A Coyote supersonic sea skimming target drones for missile defense,” Military & Aerospace Electronics. Available: <https://www.militaryaerospace.com/unmanned/article/16726736/northrop-grumman-to-build-15-gqm163a-coyote-supersonic-sea-skimming-target-drones-for-missile-defense>
- [11] Fleeman, E. L., “Tactical Missile Design”, 1st Edition, *AIAA Education Series*, AIAA, Reston, 2001.
- [12] Sutton, G. P., Biblarz, O., “Rocket Propulsion Elements”, 8th Edition, John Wiley & Sons, INC., 2010.
- [13] “Ramjet/Scramjet Thrust”, *NASA*. Available: <https://www.grc.nasa.gov/WWW/K-12/airplane/ramth.html>
- [14] Seitzman, J. M., “Oblique Shocks,” Georgia Institute of Technology, 2018. Available: <http://www.seitzman.gatech.edu/classes/ae2010/obliqueshocks.pdf>
- [15] Wilson, R. C., “Development and Validation of a Solid Rocket Motor Analysis Code,” *AE 8900 MAV Special Problems*, Georgia Institute of Technology, 2019.
- [16] Arrowood, R. H., Donnan, R. H., Goodman, J. M., Gordon, S. E., Jenista, C. G., Maschmeyer, T. M., Sanders, A. D., “High-Speed Advanced Long Range Air-to-Air Missile (HALRAAM)”, *AIAA MSTC Graduate Missile Design Competition 2013-2014*, Georgia Institute of Technology Aerospace Systems Design Laboratory, Atlanta, GA.
- [17] “ASM Specification Aerospace Metals”, (n.d.). Available: <https://www.aerospacemetals.com/>
- [18] Caywood, W. C., Rivello, R. M., Weckesser, L. B., “Tactical missile structures and materials technology”, *Johns Hopkins APL Technical Digest*, 1983.
- [19] Shippen, W. M., Berl, W. G., Garten, W., Hardgrave, E. J., JR., “The Talos Propulsion System”, *Johns Hopkins APL Technical Digest*, 1982.

- [20] Minzner, R.A., Champion, K. S. W., Pond, H. L., "The ARDC Model Atmosphere 1959", *Geophysics Research Directorate*, Air Force Cambridge Research Center, Air Research and Development Command, U.S. Air Force, Bedford, MA, 1959.
- [21] "scipy.optimize.minimize," *SciPy.org*, December, 2019. Available: <https://docs.scipy.org/doc/scipy/reference/generated/scipy.optimize.minimize.html>
- [22] "Global Positioning System Standard Positioning Service Performance Standard," Department of Defense, April 2020. Available: <https://www.gps.gov/technical/ps/2020-SPS-performance-standard.pdf>
- [23] "Selected Acquisition Report (SAR) Standard Missile-6 (SM-6) As of FY 2020 President's Budget", *Defense Acquisition Management Information Retrieval (DAMIR)*, RCS: DD-A&T(Q&A)823-391, December 2018. Available: https://www.esd.whs.mil/Portals/54/Documents/FOID/ReadingRoom/Selected_Acquisition_Reports/19-F-1098_Doc_78_SM-6_SAR_Dec_2018.pdf
- [24] "BrahMos Supersonic Cruise Missile", *Army Technology*. Available: <https://www.army-technology.com/projects/brahmossupersoniccru/>